TÜRKİYE CUMHURİYETİ
ADANA ALPARSLAN TÜRKEŞ SCIENCE AND TECHNOLOGY UNIVERSITY

GRADUATE SCHOOL
MECHANICAL ENGINEERING DEPARTMENT

EXPERIMENTAL AND NUMERICAL INVESTIGATION OF THE EFFECTS OF DIFFERENT PARAMETERS ON A STIRRED HEAT EXCHANGER EFFECTIVENESS

MAHİR ŞAHİN

M.Sc.

ADANA 2024

TÜRKİYE CUMHURİYETİ
ADANA ALPARSLAN TÜRKEŞ SCIENCE AND TECHNOLOGY UNIVERSITY

GRADUATE SCHOOL
MECHANICAL ENGINEERING DEPARTMENT

EXPERIMENTAL AND NUMERICAL INVESTIGATION OF THE EFFECTS OF DIFFERENT PARAMETERS ON A STIRRED HEAT EXCHANGER EFFECTIVENESS

MAHİR ŞAHİN

M.Sc.

THESIS ADVISOR
ASSOC. PROF. DR. MUSTAFA KILIÇ

ADANA, 2024

ÖZET

KARIŞTIRICILI BİR ISI DEĞİŞTİRİCİ ETKİNLİĞİNE FARKLI PARAMETRELERİN ETKİSİNİN DENEYSEL VE SAYISAL İNCELENMESİ

Mahir ŞAHİN
Yüksek Lisans, Makine MühendisliğiAnabilim Dalı
Danışman: Doç. Dr. Mustafa KILIÇ
Ağustos 2024, 68 sayfa

Enerji verimliliğinin artışı hem olumsuz çevresel etkilerin azaltılması hem de işletme maliyetlerinin düşürülmesi açısından önemini korumaktadır. Endüstriyel işletmelerdeki ısıl yükler, atık ısılar, enerji tüketiminde önemli bir paya sahiptir. Bu proseslerin verimli ve tasarruflu bir şekilde yürütülmesinde ısı değiştiricilerin payı büyüktür. Bu tez çalışmasında karıştırıcılı bir ısı değiştiricinde mekanik karıştırıcının dönme hızı, Reynolds sayısı, akışkan giriş sıcaklıklarının ısı transfer performansına olan etkisi deneysel olarak incelenmiştir. Hesaplamalı akışkanlar dinamiği yazılımıyla oluşturulan sayısal model doğrulandıktan sonra, karıştırıcı çark ve kanat geometrisinin ısı transfer performansıma olan etkisi incelenmiştir. Sayısal çalışmada ANSYS Fluent 2022 R1 yazılımında hareketli ağ yapısının modellenmesi için Hareketli Referans Sistemi (MRF) ve çözüm için düşük Reynolds düzeltmeli SST k-ω türbülans modeli kullanılmıştır. Sonuç olarak; çark hızının 0'dan 200 d/dk'ya kadar artırılması, ısı transfer etkinliğinde %55,1 artış, çark yüksekliğinin H=10 mm'den H=40 mm'ye artırılması ısı transfer etkinliğinde %17,2 artış, çark çapının D=40 mm'den D=100 mm'ye artırılması ısı transfer etkinliğinde %15,9 artış, kanat açısının θ=0°'dan θ=45°'e kadar artırılması ısı transfer etkinliğinde %14,4 artış, kanat sayısının n=2'den n=3'e çıkarılması ısı transfer etkinliğinde %12,6 artış ve çark sayısının S=1'den S=2'ye çıkarılması ise ısı transfer etkinliğinde %16,7 artış sağladığı tespit edilmiştir. Bu tez çalışmasından elde edilen sonuçlarla, termal proseslerde ısı değiştiricisine ait verimliliklerin artırılmasına bağlı olarak enerji tasarruflu sistemlerin geliştirileceği değerlendirilmiştir.

Anahtar Kelimeler: Isı değiştiricisi, mekanik karıştırıcı, kanat geometrisi, ısı transferi.

ABSTRACT

EXPERIMENTAL AND NUMERICAL INVESTIGATION OF THE EFFECTS OF DIFFERENT PARAMETERS ON A STIRRED HEAT EXCHANGER EFFECTIVENESS

Mahir ŞAHİN

M.Sc., Department of Mechanical Engineering

Supervisor: Assoc. Prof. Dr. Mustafa KILIÇ

August 2024, 68 pages

Increasing energy efficiency remains crucial for both reducing adverse environmental impacts and reducing operational costs. Thermal loads and waste heat in industrial operations account for a significant portion of energy consumption. Heat exchangers play a major role in running these processes efficiently and economically. In this thesis, the effects of the mechanical stirrer's rotational speed, Reynolds number, and fluid inlet temperatures on the heat transfer performance in a stirred heat exchanger were experimentally investigated. After validating the numerical model created with computational fluid dynamics software, the impact of the stirrer's impeller and blade geometry on heat transfer performance was examined. In the numerical study, the Moving Reference Frame (MRF) for modeling the moving mesh structure and the low Reynolds corrected SST k-ω turbulence model were used for the solution in ANSYS Fluent 2022 R1 software. As a result: increasing the impeller speed from 0 to 200 rpm resulted in a 55.1% increase in heat transfer effectiveness; increasing the impeller height from H=10 mm to H=40 mm resulted in a 17.2% increase; increasing the impeller diameter from D=40 mm to D=100 mm resulted in a 15.9% increase in heat transfer effectiveness; increasing the blade angle from θ=0° to θ=45° resulted in a 14.4% increase in heat transfer effectiveness; increasing the number of blades from n=2 to n=3 resulted in a 12.6% increase in heat transfer effectiveness; and increasing the number of impellers from S=1 to S=2 resulted in a 16.7% increase in heat transfer effectiveness. The results of this thesis suggest that improving the efficiency of heat exchangers in thermal processes can lead to the development of more energy-efficient systems.

Keywords: Heat exchanger, mechanical stirrer, blade geometry, heat transfer.

Dedication

"To my beloved father who never loses hope in my success..."

ACKNOWLEDGEMENTS

I would like to extend my heartfelt gratitude to my esteemed advisor, Assoc. Prof. Dr. Mustafa KILIÇ, whose expertise, dedication, and unwavering support have been instrumental in the completion of this thesis.

Dr. KILIÇ, your profound knowledge in the field of thermodynamics and heat transfer has been a guiding light throughout this journey. Your insightful feedback and constructive criticism have significantly enhanced the quality of my work. I am deeply grateful for the countless hours you have dedicated to mentoring me, from meticulously reviewing my drafts to providing me with the necessary tools and resources to succeed.

Your encouragement and belief in my abilities have been a constant source of motivation. You have not only guided me academically but also inspired me to strive for excellence in all my endeavors. The skills and knowledge I have gained under your mentorship will undoubtedly shape my future career.

Thank you, Dr. KILIÇ, for your patience, wisdom, and unwavering support. It has been an honor to work under your supervision, and I am sincerely appreciative of all that you have done to help me reach this milestone.

TABLE OF CONTENTS

LIST OF FIGURES

LIST OF TABLES

LIST OF ABBREVIATIONS

ANN	: Artificial Neural Network
PCM	: Phase Chage Material
Ne-PCM	: Nano-Enhanced Phase Chage Material
STHE	: Shell-Tube Heat Exchanger
LMTD	: Logarithmic Temperature Difference
CFD	: Computational Fluid Dynamics
MRF	: Moving Reference Frame
SST	: Shear Stress Transport
AISI	: American Iron and Steel Institute
FBDT	: Flat Blade Disc Turbine
DEM	: Discrete Element Method
PIV	: Particle Image Velocimetry
SWT	: Solar Water Tank
PHE	: Plate Heat Exchanger
RANS	: Reynolds Average Navier Stokes
DEM	: Discrete Element Method

LIST OF SYMBOLS

Nu	: Nusselt number
Re	: Reynolds number
U_r	: Radial velocity
U_θ	: Tangential velocity
U_z	: Axial velocity
ΔT_{lm}	: Logarithmic mean temperature difference
ε	: Heat transfer effectiveness
υ	: Kinematic viscosity
μ	: Dynamic viscosity
D	: Diameter of impeller
H	: Height of impeller
θ	: Angle of impeller
n	: Number of blades
S	: Number of stirrers
$T_{h,in}$	: Hot fluid inlet temperature
$T_{c,in}$	: Cold fluid inlet temperature
$T_{h,out}$	: Hot fluid outlet temperature
$T_{c,out}$	: Cold fluid outlet temperature
imp	: Impeller

1. INTRODUCTION

The rise in energy consumption has prompted researchers and engineers to explore a variety of energy sources and develop methods to reduce energy use. In many industrial plants today, the increasing heat load has drawn the attention of researchers in terms of energy savings. The effective operation of heat exchangers in thermal processes highlights a critical area of research that demands attention. Heat exchangers are widely used in the fields of chemistry, metallurgy, food processing, pharmaceuticals, and many other manufacturing sectors (Hu & Heiselberg, 2018; Zhang et al., 2024). Depending on their diverse applications, heat exchangers come in various types and specifications. In the literature, the most studied heat exchangers are double pipe and shell and tube heat exchangers (Hosseini et al., 2014; Mase et al., 2024; Parsa et al., 2024; Safari et al., 2024). Mechanically stirred-jacketed heat exchangers have been studied less compared to other types. The need for an external energy source to operate the stirrer element in stirred heat exchangers has led to their less frequent use, resulting in a limited number of studies in this area. Improving the design and efficiency of stirred-jacketed heat exchangers is crucial for energy savings and more effective heat transfer.

1.1. Design Parameters

Key factors for designing agitated tanks and stirred heat exchangers include vertical cylindrical containers, impellers, wall baffles, inlets, and outlets. Agitated tanks used as heat exchangers are known in the literature as agitated jacketed heat exchangers (Mahir et al., 2021; Mohan Anthony Nicholas Emery Tariq AI-Hassan, 1992). Impellers are very significant design parameters in agitated heat exchangers for improving heat transfer efficiency. There are two types of methods for improving heat transfer performance: passive methods and active methods. Integrating an agitator in a heat exchanger is an active way for improving heat transfer performance.

1.1.1. Different Types of Impellers

In commercial settings, a wide range of impeller types are used, with the best choice depending on the process requirements and material properties. Impellers are divided into two types: turbines for fluids with low to medium viscosity and close-clearance impellers for high viscosity fluids. Turbine impellers are further defined by their flow patterns, which might be axial or radial. Axial and radial impellers differ in terms of the direction of fluid flow (Paul et al., 2004a). Radial impellers discharge perpendicular to the axis of rotation, whereas axial impellers discharge parallel to it. Under particular conditions, both kinds can discharge in the opposite way. Impellers are also classed according to the mixing flow regime, which is either laminar or turbulent. Laminar impellers are smaller and try to disperse fluid throughout the tank using low fluid momentum (Allison et al., 2011). Turbulent impellers are bigger and classed according to their function: flow, pressure, or shear. Typical impellers for axial flow radial flow are showed in Figure 1.1.

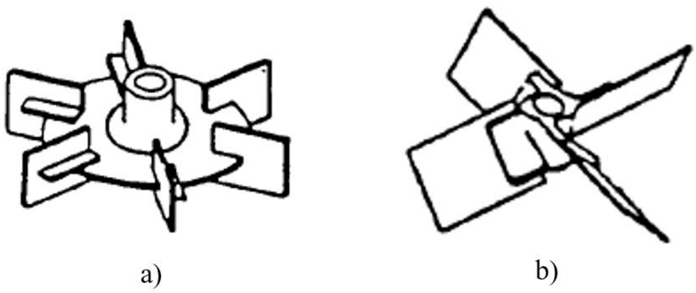

Figure 1.1. Typical impellers for a) axial flow b) radial flow (Rezend, 1996a)

1.1.2. Mixing Tanks

A standard stirred tank is a cylindrical vessel containing a spinning mixer, which is often used for mixing operations. While cylindrical vessels are most common, square or lateral cylinders are also used on occasion. The mixer's components include an impeller, drive shaft, gearbox, and motor output. In bigger tanks, the mixer can be placed near the bottom to minimize shaft length and improve mechanical stability (Sui et al., 2024). A general example of stirred tank is presented in Figure 1.2.

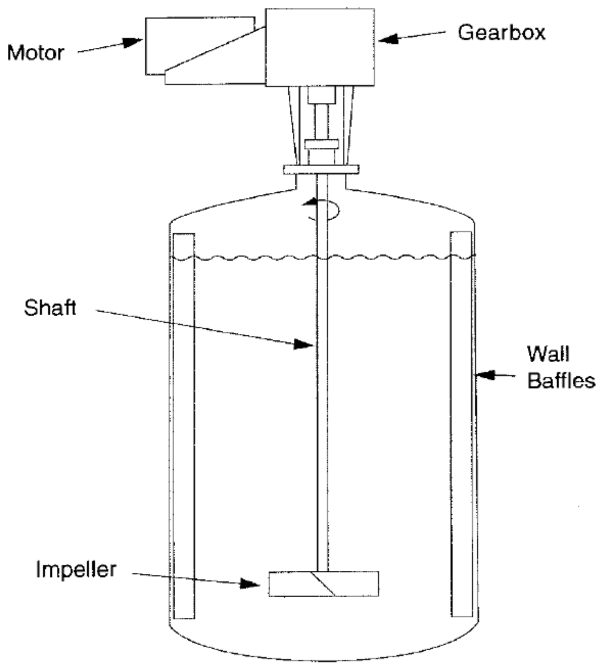

Figure 1.2. A typical stirring tank with base components. (Paul et al., 2004b)

1.1.3. Baffles and Turbulators

Turbulators and wall baffles are frequently used to facilitate efficient mixing by inhibiting solid body motion and increasing axial blending among the top and bottom of the vessel. Their presence has a major impact on flow dynamics and, consequently, mixing efficiency (Abolpour et al., 2021; Alwatban & Aljabr, 2024). Without baffles and turbulators, impeller rotation results in a two-dimensional flow with swirling motion or solid body rotation. Wall baffles decrease air entrainment by channeling tangential flows into vertical ones, allowing for smooth top-to-bottom mixing. However, baffles increase the impeller's drag and power consumption.

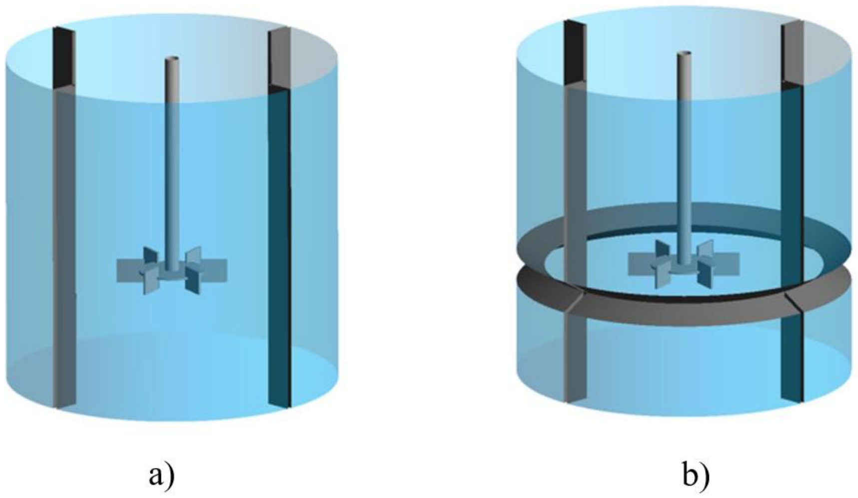

Figure 1.3. Geometrical structures of the a) wall baffles and b) V-shaped baffles (Shen et al., 2021)

In mixing tanks, baffles that affect mixing dynamics can be implemented in various configurations. Shen et al. (2021) investigated the impact of different configurations of wall baffles and V-shaped baffles at various angles on flow characteristics in a mixing tank. The tank geometries created are presented in Figure 1.3.

1.2. Heat Transfer Mechanism

Conduction and convection are the primary heat transfer processes in stirred tanks and stirred heat exchangers. Conduction occurs in heat exchangers through the solid walls as well as the impeller or stirring element surfaces. The thermal conductivity of these materials contributes significantly to heat transmission from the heat source to the fluid within the heat exchanger. In these systems, mechanical stirrers dramatically improve convective heat transfer (Gulumyan et al., 2017). The impeller's spin causes fluid velocity, resulting in a forced convection environment. This improves fluid mixing, resulting in consistent temperature distribution and increased total heat transfer efficiency. The impeller creates turbulent flow inside the fluid. This turbulence disperses thermal boundary layers that occur near heated or cooled surfaces, enhancing the heat transfer coefficient. The impeller's better mixing reduces hot and cold patches, resulting in a more uniform temperature profile throughout the fluid.

1.2.1. Thermal Conductivity and Material Selection

In a jacketed heat exchanger, the system's biggest resistance determines the overall heat transfer coefficient. Fouling on either the heat transfer fluid or the process fluid side can drastically reduce heat transfer. For carbon steel containers, the wall conductivity is usually strong, hence conductive resistance is just a tiny component of overall heat resistance. However, in stainless steel and glass-lined containers, reduced thermal conductivity can have a considerable impact on the total heat transfer coefficient (Paul et al., 2004b). The most researched types of materials for stirred heat exchangers in the literature are presented in Table 1.

Table 1. Different types of materials for stirred heat exchangers

Material	**Thermal Conductivity, k [W/m·K]**	**Specific Heat, C_p [J/kg·K]**	**Density, ρ [kg/m³]**
Carbon steel	52	460	7800
Copper	377	385	9000
Cupro-nickel 90/10	52	444	8700
Cupro-nickel 70/30	35	444	8300
Glass	1.16	835	2500
Hastelloy C276	11	385	8900
Incoloy 825	12	512	8100
Inconel 600	16	444	8300
Monel (400, 404, R405, 411)	26	427	8800
Nickel (200, 201, 220, 225)	66	440	8900
Stainless steel (304, 316, 321, 347)	17	502	7700
Tantalum	54	151	16600
Titanium	20	582	4500

1.2.2. Flow Characteristics

In describing the flow characteristics generated by impellers in a stirred heat exchanger, flow patterns, pumping, and shear are critical factors. The mixing process is significantly influenced by impeller flow patterns. Axial flow impellers, such as propellers and pitched blade turbines, produce a single circulation loop throughout the tank, offering a good balance of pumping and shear (Petera et al., 2016). Radial flow impellers create two circulating loops, one above and one below the impeller, leading to compartmentalized mixing. The choice of impeller depends on the required flow patterns and shear rates, with axial flow being effective for liquid blending and radial flow for gas dispersion. The flow patterns can be modified by impeller diameter, liquid viscosity, and the use of multiple impellers. Additionally, effective blending in large tanks can be achieved with side-entering propeller mixers positioned slightly off-center to avoid surface vortexing and improve blending efficiency.

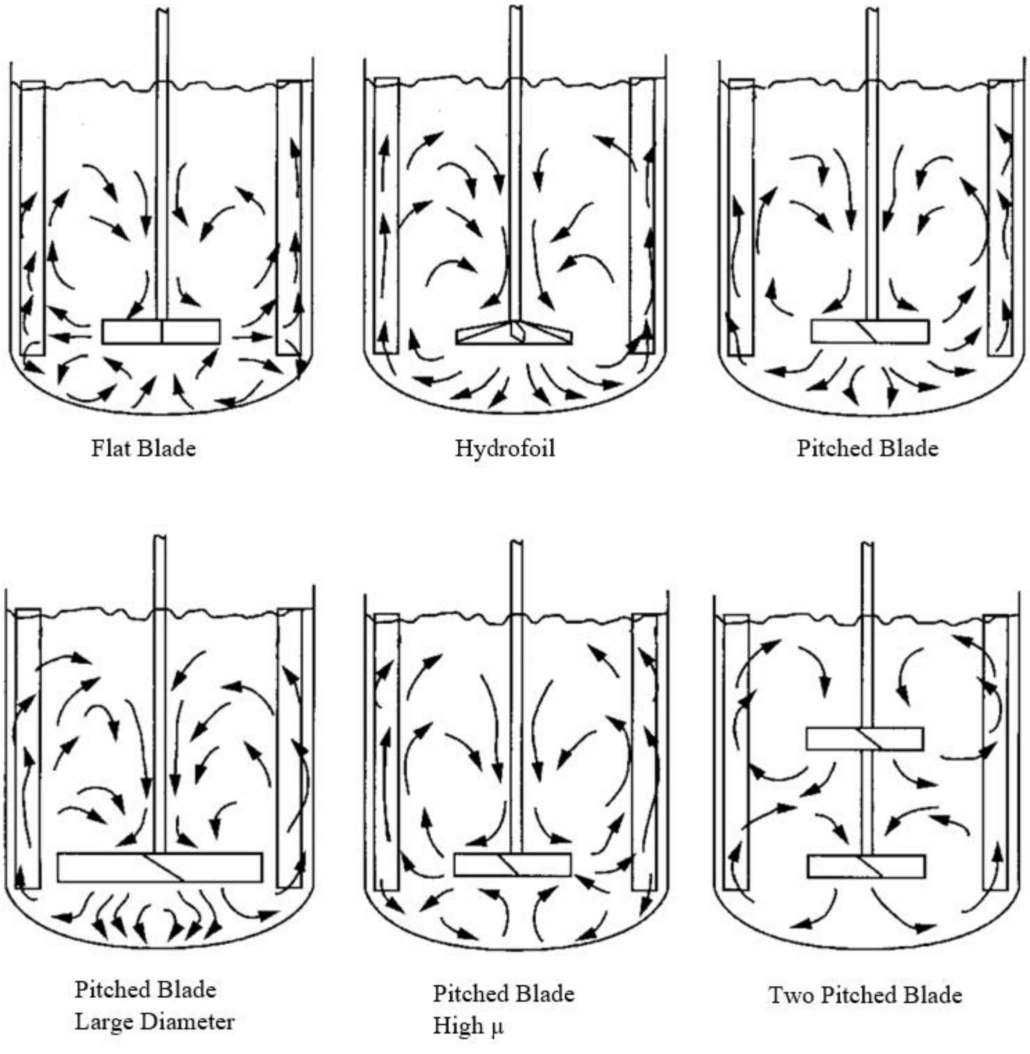

Figure 1.4. Flow patterns for different impeller types (Paul et al., 2004b)

The relative motion of liquid layers generates shearing forces linked to flow velocities, resulting in fluid intermixing, dispersing gas bubbles, and breaking liquid droplets (Nobuo Mitsuishi, 1973). These forces, represented by shear stress, vary with shear rate, impeller blade pressure drop, turbulence level, and viscosity. Velocity gradients between neighboring material sections result in shearing and dispersion (Joshi et al., 2011). Time-averaged velocities near the impeller blade may be used to calculate macroflow velocity gradient and shear rate.

In multiple-impeller systems, impeller clearance from the tank bottom and spacing have a substantial impact on power, flow patterns, and process outputs. These effects vary depending on the mixing mechanism and requirements. Down-pumping axial flow impellers at the tank bottom can produce radial flow patterns, resulting in less pumping and more shear, which may assist maintain the tank bottom free of solids but lower bulk homogeneity.

2. LITERATURE REWIEW

Mechanically stirred devices are essential in industrial applications because they offer operational flexibility and versatility. Stirred tanks are widely used in a variety of process industries, including food, chemicals, petrochemicals, pharmaceuticals, and textiles, where they serve as reactors, heat exchangers, evaporators, storage containers, and more. These containers often have jacketed systems designed to circulate liquid or steam, allowing for the controlled transmission of heat at a certain flow rate and temperature.

Essentially, the purpose is to guarantee that the fluids in these tanks attain the appropriate qualities, such as temperature and homogeneity, within a set time limit. The impellers in the tank are critical for determining how long it takes to attain the required conditions. Tank size, stirrer placement and number, distance between the stirrer and the tank's bottom, baffle type, and wall thickness are all factors that influence the thermal efficiency and processing time of a jacketed heat exchanger with a stirrer (Rezend, 1996b). Thermal efficiency and processing time are further influenced by mass flow rate, temperature differential across the separating wall for hot and cold fluids, and stirrer rotating velocity (Sevilgen & BAYRAM, 2018). According to research, adding baffles around the tank's inner sides can help to reduce undesired vortexes.

Karagoz et al. (2017) used experimental and computational methods to investigate the effects of gaps between cylindrical blade constructions, blade angles, and Reynolds numbers in turbulent flow conditions within stirred heat exchangers. Their findings demonstrated that the Nusselt number and friction factor rose as the effective diameter dropped. Furthermore, it was determined that adjustments in blade angle did not result in significant changes in the Nusselt number or friction factor, with the findings being rather constant.

Zhao et al. (2022) have examined the important geometric parameters for a high-energy efficiency mixer tank through fluid dynamics calculations using Artificial Neural Network (ANN). In the stirrer tank, cup-shaped blades have been investigated with respect to different configurations of blades. Analyses using ANN modeling reveal the complex and interdependent impacts of geometrical factors on energy consumption and flow characteristics.

Fouad et al. (2013) studied impeller rotation speed, cylinder diameter, cylinder spacing within the array, distance between the array and the tank wall, impeller shape (radial flow turbine and axial flow turbine) and superimposed axial solution flow in agitated vessels. The study found that the radial flow turbine had higher rates of mass transfer than the axial flow turbine. The relevance of these discoveries was highlighted in terms of the design and operation of catalytic stirred tank reactors with built-in heat transfer capabilities. Such reactors are judged appropriate for diffusion-controlled exothermic processes that need quick cooling to protect heat-sensitive catalysts and products.

Khan (2024) explored heat diffusion and mixing effects in food processing, using a non-classical continuity approach to better model liquid food flows. Applying Cosserat continuum theory, numerical simulations via the finite element method analyzed heat transfer with various mixer settings. The study found that faster particle rotations increased temperature differences at tank walls and improved mixing efficiency, while higher Cosserat numbers dispersed vortices, affecting temperature differences and particle mixing dynamics. Jaehrling & Schultz (2019) examined the impact of various heat exchanger components and reactor base shapes on heat transfer and flow characteristics. They used stereo PIV measurements in optically clear systems to highlight specific advantages and disadvantages of each configuration, emphasizing their significant effects on heat transfer efficiency and overall flow patterns within mixed vessels. Srinivas & Venu Vinod (2015) performed an experimental examination of stirred tanks and helical coils, with an emphasis on forced convection heat transfer. They employed CuO nanoparticle combinations in water with varying concentrations, mixing rates, and tank temperatures. The findings describe how these factors affect the heat transfer rate. Di Bari et al. (2014) investigated the emulsification processes in the margarine production process and discovered a clear association between crystallization behavior and mechanical shear. The work enhanced emulsion stability and process optimization in similar industrial applications by fitting droplet size data to a power law model, which is extensively utilized in the literature for high-shear mixers. Rasslan et al. (2023) studied the heat and mass transfer parameters of a serpentine tube heat exchanger mounted on the wall of a square stirred tank reactor using electrochemical measuring methods. The study looked at the effects of factors such propeller rotation speed, geometry, pipe diameter, and pipe pitch. The findings revealed that mass and heat transfer coefficients rose with greater propeller speeds but dropped with bigger cylinder diameters and pitches. Dhaou et al. (2022) investigated the performance of a solar water tank (SWT) equipped with a nano-enhanced phase change material (Ne-PCM) and a stirrer. SWT/Ne-PCM was created and developed in two configurations: spiral and jacketed tube heat exchangers. These SWTs were combined with nano-enhanced PCM in cylindrical capsules, and a laboratory-scale experimental setup was built to test their performance impact. The findings

revealed that, as compared to a jacketed tank (without mixing), SWT/Ne-PCM operations (with stirrer and coil) reduced loading and unloading durations by 12.5% and 23.51%, respectively.
Srinivas & Venu Vinod (2013) examined the energy efficiency of a shaken helical coil heat exchanger using Al_2O_3/water nanofluid to standard water as the heating medium. Several factors, including nanofluid concentration, flow rates, mixing speeds, and shell-side fluid temperatures, were studied. The results revealed that energy savings were more obvious during laminar and turbulent flow conditions compared to the transitional regime. The percentage of energy savings increased with the concentration of Al_2O_3 nanoparticles. Norton & Fryer (2012) investigated critical factors such as polyglycerol polyricinoleate (PGPR) concentration, emulsion characteristics, tempering, polymorphic forms, and uses in chocolate. The study revealed the possibility and advantages of employing cocoa butter emulsions made using this technology to increase chocolate production efficiency and quality, as well as potentially lower fat content without sacrificing product quality. Niedbalski et al. (2014) studied the hydrodynamic behavior of gas-evolving reactive fluxes in chevron plate heat exchangers (PHEs). Chevron plate heat exchangers were compared to traditional heat exchanger/reactor designs, and a correlation test was performed Srinivas & Venu Vinod (2016) investigated the performance of a shaken shell and helical coil heat exchanger using water-based nanofluids (Al_2O_3, CuO, and TiO_2). The experiment analyzed the impact of various nanofluid concentrations (Al_2O_3, CuO, and TiO_2), temperatures, mixing speeds, and liquid flow rates on the coil side. The results revealed that employing nanofluids improved the heat exchanger's efficacy compared to using merely water. Results indicated a maximum increase of 30.37% with Al_2O_3/water nanofluid, 32.7% with CuO/water nanofluid, and 26.8% with TiO_2/water nanofluid.
Cui et al. (2018) performed experimental and numerical studies on the mixing process in pitched-blade turbine stirred tanks with laminar flow. Their findings revealed that, among the characteristics tested, impeller diameter had the greatest impact on mixing time. Following impeller diameter, the criteria influencing mixing time in descending order were discharge angle and blade width.
The heat transfer coefficient and volumetric energy density were measured in a coiled stirred tank filled with a low-cost Phase Change Material (PCM) emulsion. Their findings showed that when the stirring rate was between 290 and 600 rpm, the total heat transfer coefficient rose by around 3.5-5.5 times (Delgado et al., 2017).

Debab et al. (2011) performed experiments in a jacketed tank fitted with turbine impellers to establish the ideal experimental conditions for a non-Newtonian liquid. Based on the optimization results, they found that an agitated vessel with a Flat Blade Disc Turbine (FBDT) with a diameter ratio of 0.6 and baffles had the best heat transmission qualities. A computational fluid dynamics (CFD) model was created for a jacketed stirred tank equipped with a six-blade Rushton turbine impeller with the goal of establishing a Nusselt number correlation. This link was sought since the heat transfer coefficient is dependent on the impeller and its rotating speed (Daza et al., 2019).

B. Lakghomi (2006) claimed that the Nusselt number correlation results closely matched the experimental data, indicating a valid depiction of heat transmission within the tank. Numerical analyses of the effects of stirring coils and jackets were conducted on flow behaviors and heat transfer within tanks. Observations revealed that using coils resulted in a more equal temperature distribution and a higher heat transfer coefficient. However, it should be noted that the power required for impellers was larger in coiled stirred tanks than in jacketed ones.

Soliman et al. (2017) investigated an exothermic liquid-solid diffusion-controlled catalytic reaction in a stirred reactor tank. The variables evaluated were impeller rotation speed, impeller shape, solution physical characteristics, and serpentine tube baffle width.

Luo et al. (2021) studied CFD-DEM coupling model to investigate particle fluxes, which include both momentum exchange and heat convection. To analyze the influence of particles on temperature distribution in stirred tanks, a comparative study of computed temperature distributions is performed, considering both liquid-solid flow and single-phase flow. The study found that radial flow has a significant role in heat transmission in stirred tanks with particle fluxes. Furthermore, the wide dead zone reduces particle temperature homogeneity and heat transmission efficiency. Thus, increasing the radial flow and eliminating the dead zone are critical for improving heat transfer efficiency in stirred tanks with particle fluxes.

Kisuka et al. (2023) performed experimental work used a mechanical stirred tank to combine grains. This study looked at how different factors affected temperature distributions. It was discovered that increasing rotation speed, fill ratio, and particle size results in higher temperature increases. Furthermore, flat blades produced more heat than slanted blades.

After a comprehensive literature review, numerous studies have been found investigating heat exchangers. However, the number of studies examining jacketed heat exchangers with stirrer is quite limited. In this thesis, unlike the studies in the literature, the effect of Reynolds number

based on fluid velocity, impeller rotation speed, and inlet temperature on heat transfer performance in a stirred jacketed heat exchanger was experimentally investigated. Subsequently, a numerical model created using computational fluid dynamics software was validated with experimental data. After validation, the effects of impeller rotation speed, impeller height in the tank, impeller diameter, impeller blade angle, blade number, and impeller number on the heat transfer performance of the heat exchanger were examined. The results obtained from this thesis aim to enable systems using stirrer heat exchangers to operate more efficiently and establish more cost-effective systems.

3. MATERIALS AND METHODS

The thesis work was conducted through both experimental and numerical approaches to ensure comprehensive analysis and validation of results. The experimental investigations were meticulously carried out in the Heat Transfer and Thermodynamics Laboratory at Adana Alparslan Türkeş Science and Technology University. This facility is equipped with instrumentation and technology to accurately measure and analyze heat transfer phenomena. Following the completion of the experimental phase, a detailed numerical study was undertaken using ANSYS 2022 R1 software. This involved creating a precise computational model to simulate the experimental conditions and validate the experimental findings. The integration of experimental and numerical methods provided a robust framework for understanding the effects of various parameters on the performance of the stirred heat exchanger.

3.1. Experimental Setup

The jacketed stirrer heat exchanger, and its shaft and blades of the stirrer are made of stainless steel AISI 304. The diameter of the tank section is 105 mm, and its length is 145 mm. The diameter of the jacket section is 135 mm, and its length is 127 mm. The mechanical stirrer is 3-bladed and enable to operate in the range of 0-330 rpm for rotational motion. Figure 3.1. shows an image of the heat exchanger.

Figure 3.1. The jacketed stirred heat exchanger used in the experimental study

The heat exchanger is integrated with the experimental module to enable a comprehensive range of measurements and observations. This setup allows for the precise monitoring of the inlet and outlet temperatures of both the hot and cold fluids, providing critical data on the thermal performance and efficiency of the heat exchange process. Additionally, the rotational speed of the stirrer is measured to ensure optimal mixing and uniformity of the fluid temperatures. The system also includes instrumentation to accurately measure the flow rates of the fluids, which is essential for analyzing the heat transfer rates and determining the overall effectiveness of the heat exchanger. This setup ensures that all relevant parameters are closely monitored, facilitating detailed analysis and optimization of the heat exchange process. The experimental module is presented in Figure 3.2. This module, which includes a hot water tank and a circulation pump, enables the continuous transfer of hot fluid to the heat exchanger.

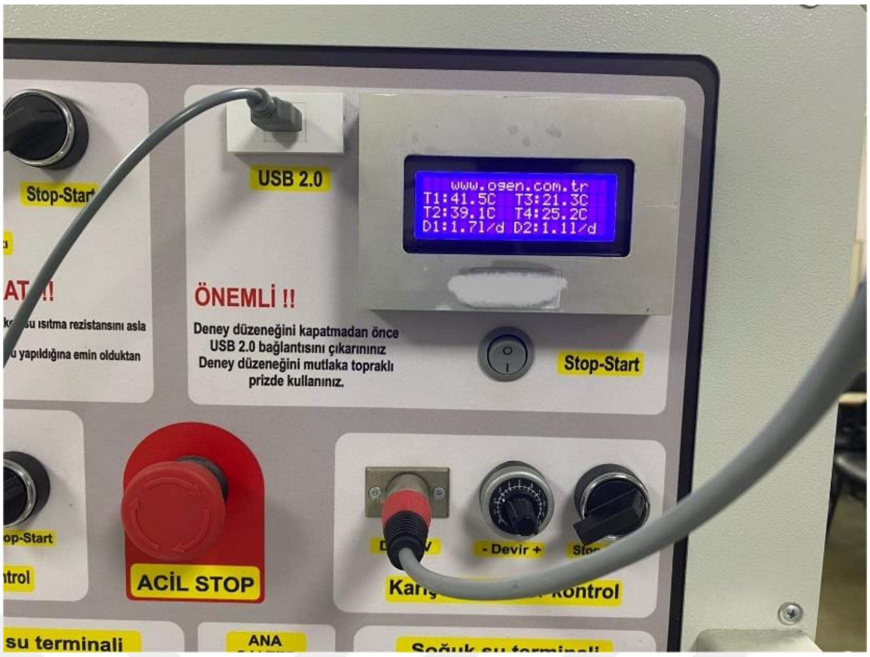

Figure 3.2. The experimental module where the fluid properties are measured

Once the fluid flow reached a steady state, ensuring steady-state conditions, a series of measurements were meticulously recorded using a data logger (Figure 3.3.). This device was employed to capture a range of critical parameters, including the inlet and outlet temperatures of the fluids, the rotational speed of the stirrer, and the flow rates of the fluids.

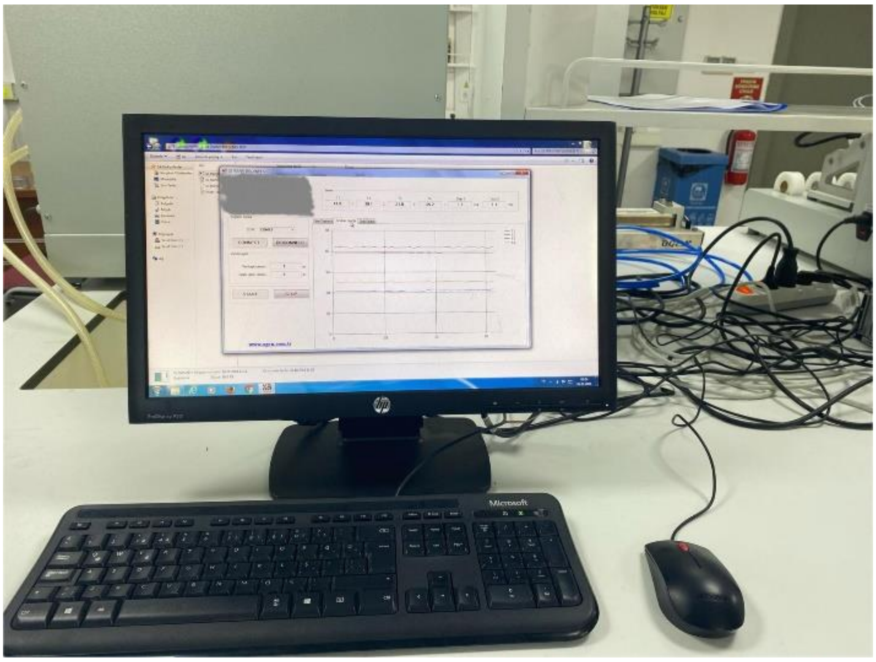

Figure 3.3. The data logging computer for the experimental study

The data logger ensured high precision and accuracy in recording these measurements over time, allowing for detailed analysis and validation of the heat exchanger's performance. A schematic diagram explaining the experimental procedure is presented in Figure 3.4.

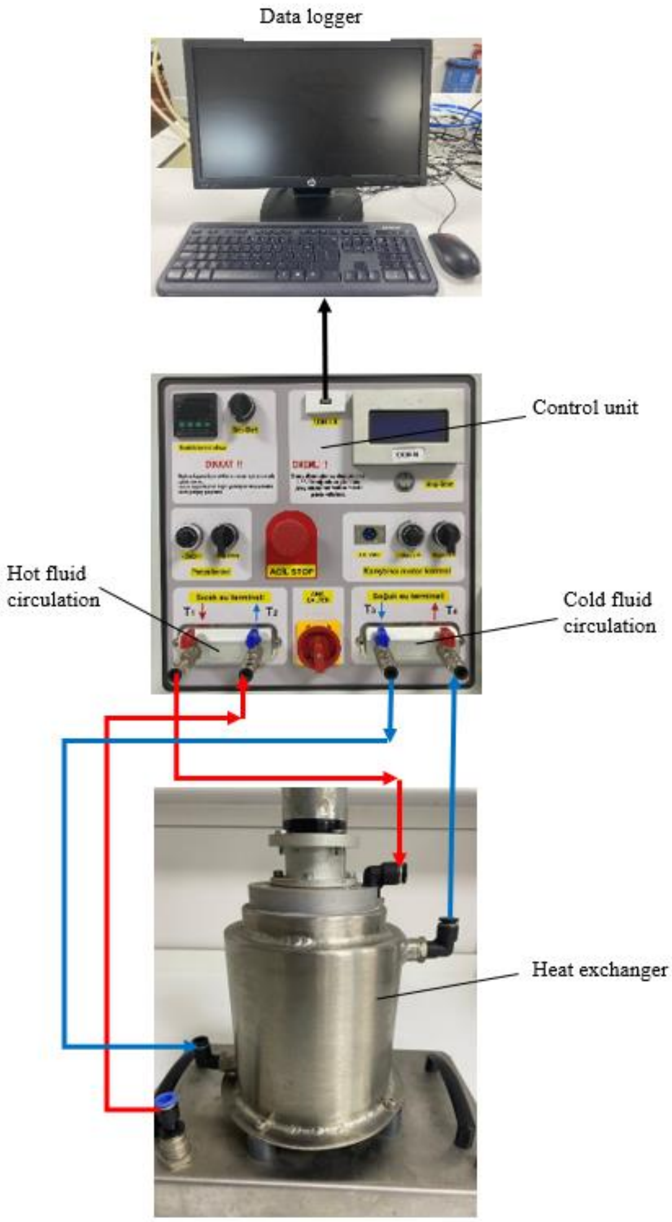

Figure 3.4. The experimental procedure of the setup

The parameters used in the experimental study are critical for assessing the heat exchanger's performance. These include the stirrer rotational speed, which affects mixing intensity and heat transfer effectiveness, the fluid Reynolds number, and the fluid inlet temperature. By systematically varying these parameters, the study aims to understand their effects on the heat transfer performance and optimize the heat exchanger design and operation.

3.2. Mathematical Formulation

The governing equations of the problem, along with the heat transfer equations, are thoroughly presented and detailed. These equations form the foundation of the numerical analysis and are crucial for accurately modeling the thermal and fluid dynamics within the heat exchanger. The governing equations typically include the continuity equation, momentum equations, and energy equation, which describe the conservation of mass, momentum, and energy, respectively.

3.2.1. Governing Equations

When examining a small volume or part of fluid in movement two changes are likely to occur: (1) the fluid element will move and even rotate in space, and (2) it will deform, either through simple expansion along multiple axes or through angular distortion leading to a change in form (Paul et al., 2004c). A sequence of conservation or transport equations is used to explain a wide range of processes, including those involving generalized fluid motion. These equations track the development of fluid properties over time, including changes produced by convection, diffusion, and the addition or removal of a preserved or transported component. The problem was approached and solved under steady-state conditions to ensure a comprehensive analysis. This involved assuming that the system's variables, such as temperature, pressure, and velocity, remained constant over time, allowing for a more accurate and stable solution.

The continuity equation states that mass is conserved. To understand its case, examine the fluid flow with density ρ through the cylindrical volume element. The continuity equation (Y. Cengel & Cimbala, 2014);

$$\frac{1}{r}\frac{\partial(ru_r)}{\partial r} + \frac{1}{r}\frac{\partial(u_\theta)}{\partial \theta} + \frac{\partial(u_z)}{\partial z} = 0 \qquad (3.1)$$

The momentum equation states that momentum is conserved in each of the three component directions. The momentum equations in r, θ, z directions are expressed as (Y. Cengel & Cimbala, 2014);

In the r-direction:

$$\rho\left(u_r\frac{\partial u_r}{\partial r}+\frac{u_\theta}{r}\frac{\partial u_r}{\partial \theta}-\frac{{u_\theta}^2}{r}+u_z\frac{\partial u_r}{\partial z}\right)=$$

$$-\frac{\partial P}{\partial r}+\rho g_r+\mu\left[\frac{1}{r}\frac{\partial}{\partial r}\left(r\frac{\partial u_r}{\partial r}\right)-\frac{u_r}{r^2}+\frac{1}{r^2}\frac{\partial^2 u_r}{\partial \theta^2}-\frac{2}{r^2}\frac{\partial u_\theta}{\partial \theta}+\frac{\partial^2 u_r}{\partial z^2}\right] \quad (3.2)$$

In the θ-direction:

$$\rho\left(u_r\frac{\partial u_\theta}{\partial r}+\frac{u_\theta}{r}\frac{\partial u_\theta}{\partial \theta}+\frac{u_\theta u_r}{r}+u_z\frac{\partial u_\theta}{\partial z}\right)=$$

$$-\frac{1}{r}\frac{\partial P}{\partial \theta}+\rho g_\theta+\mu\left[\frac{1}{r}\frac{\partial}{\partial r}\left(r\frac{\partial u_\theta}{\partial r}\right)-\frac{u_\theta}{r^2}+\frac{1}{r^2}\frac{\partial^2 u_\theta}{\partial \theta^2}+\frac{2}{r^2}\frac{\partial u_r}{\partial \theta}+\frac{\partial^2 u_\theta}{\partial z^2}\right] \quad (3.3)$$

In the z-direction:

$$\rho\left(u_r\frac{\partial u_z}{\partial r}+\frac{u_\theta}{r}\frac{\partial u_z}{\partial \theta}+u_z\frac{\partial u_z}{\partial z}\right)=-\frac{\partial P}{\partial z}+\rho g_z+\mu\left[\frac{1}{r}\frac{\partial}{\partial r}\left(r\frac{\partial u_z}{\partial r}\right)+\frac{1}{r^2}\frac{\partial^2 u_z}{\partial \theta^2}+\frac{\partial^2 u_z}{\partial z^2}\right] \quad (3.4)$$

The energy equation is often a balancing equation that accounts for heat transport rates into and out of a system, along with any internal heat generation or consumption. The energy equation is expressed as (Y. A. Cengel & Ghajar, 2020);

$$u_r\frac{\partial T}{\partial r}+\frac{u_\theta}{r}\frac{\partial T}{\partial \theta}+u_z\frac{\partial T}{\partial z}=\frac{\dot{q}_g}{c_p}+\alpha\left[\frac{1}{r}\frac{\partial}{\partial r}\left(r\frac{\partial T}{\partial r}\right)+\frac{1}{r^2}\ \frac{\partial^2 T}{\partial \theta^2}+\frac{\partial^2 T}{\partial z^2}\right]+\frac{\phi}{\rho c_p} \quad (3.5)$$

The SST k-omega low Reynolds correction model uses Reynolds-Averaged Navier-Stokes (RANS) equations to calculate viscosity and k (turbulence kinetic energy) and omega (dissipation rate) coefficients. In this model, low Reynolds correction is used to achieve good results. The SST k-omega model is described as follows (Y. Cengel & Cimbala, 2014):

k equation can be described as follows:

$$\frac{\partial(\rho k)}{\partial x_i}(u_i k) = P_k - \beta^* \rho k \omega + \frac{\partial}{\partial x_i}\left[(\mu + \sigma_k \mu_t)\frac{\partial k}{\partial x_i}\right] \tag{3.6}$$

ω equation can be described as follows:

$$\frac{\partial(\rho \omega)}{\partial x_i}(u_i \omega) = \frac{\gamma\rho}{\mu_t}P_k - \beta\rho\omega^2 + \frac{\partial}{\partial x_i}\left[(\mu + \sigma_\omega \mu_t)\frac{\partial \omega}{\partial x_i}\right] + 2(1 - F_1)\rho\sigma_{\omega 2}\frac{1}{\omega}\frac{\partial k}{\partial x_i}\frac{\partial \omega}{\partial x_i} \tag{3.7}$$

ρ fluid density, u_i velocity component, μ dynamic viscosity, μ_t turbulence viscosity, ω turbulence dissipation rate, F_1 damping function, τ_{ij} Reynolds stress tensor, v kinematic viscosity and $\beta = 0.075$, $\beta^* = 0.09$, $\gamma = 5/9$, $\sigma_k = 2$, $\sigma_\omega = 2$, $\sigma_{\omega 2} = 1$ are constants for the turbulence model.

$\frac{\gamma\rho}{\mu_t}P_k$ denotes turbulence kinetic energy production term, $\beta\rho\omega^2$ turbulence dissipation rate destruction term, $\frac{\partial}{\partial x_i}\left[(\mu + \sigma_k \mu_t)\frac{\partial \omega}{\partial x_i}\right]$ diffusion term, $2(1 - F_1)\rho\sigma_{\omega 2}\frac{1}{\omega}\frac{\partial k}{\partial x_i}\frac{\partial \omega}{\partial x_i}$ Cross-Diffusion term for low Reynolds region.

Turbulence viscosity ;

$$\mu_t = \frac{\rho k}{\omega} \tag{3.8}$$

and turbulence kinetic energy production term;

$$P_k = \tau_{ij}\frac{\partial u_i}{\partial x_i} \tag{3.9}$$

Low Reynolds correction ensures accurate modeling of turbulence characteristics near the wall, and damping functions are used in these models. The damping function F_1 takes values close to 1 in regions where wall functions are used, and values close to 0 in the resolution regions.

$$F_1 = tanh\left[\left(\min\left(\frac{\sqrt{k}}{\beta^* \omega y}, \frac{500v}{y^2 \omega}\right)\right)^4\right] \tag{3.10}$$

3.2.2. Heat Transfer Calculations

The rate of heat transfer between the hot and cold fluids can be expressed using the overall heat transfer coefficient, which takes into account both the convective heat transfer coefficients of the fluids and the conductive resistance of the exchanger material. The effectiveness of this heat transfer process is influenced by several factors, including the temperature difference between the fluids, the flow rates, and the properties of the fluids.
Reynolds number (Y. A. Cengel & Ghajar, 2020):

$$Re = \frac{u_0 D_h}{v} \tag{3.11}$$

where; u_0 inlet velocity of the hot and v kinematic viscosity fluid.
The equations specified below are used in the calculation of the heat transfer rate of the hot and cold working fluids (Y. A. Cengel & Ghajar, 2020).

$$\dot{Q}_{cold} = \dot{m}_c c_{pc}\left(T_{c,out} - T_{c,in}\right) \tag{3.12a}$$

$$\dot{Q}_{hot} = \dot{m}_h c_{ph}\left(T_{h,in} - T_{h,out}\right) \tag{3.12b}$$

Heat capacities of hot and cold fluids (Y. A. Cengel & Ghajar, 2020);

$$C_h = \dot{m}_h c_{ph} \tag{3.13a}$$

$$C_c = \dot{m}_c c_{pc} \tag{3.13b}$$

Thus, considering the heat capacities, the heat transfer rates of the cold and hot fluid are (Y. A. Cengel & Ghajar, 2020);

$$\dot{Q}_{cold} = C_c\left(T_{c,out} - T_{c,in}\right) \tag{3.14a}$$

$$\dot{Q}_{hot} = C_h\left(T_{h,in} - T_{h,out}\right) \tag{3.14b}$$

The temperature difference between the two fluids decreases from ΔT_1 at the entrance to ΔT_2 at the output. The arithmetic mean temperature, $\Delta T_{am}=(\Delta T_1+\Delta T_2)/2$, is often used as a standard metric for average temperature differentials. The logarithmic mean temperature difference (ΔT_{lm}) accurately represents the average temperature difference between hot and cold fluids by tracing the temperature distribution of the fluids along the heat exchanger. It properly depicts the exponential fall in the local temperature difference (Y. A. Cengel & Ghajar, 2020).

$$\Delta T_{lm} = \frac{\Delta T_1 - \Delta T_2}{\ln\left(\Delta T_1/\Delta T_2\right)} \tag{3.15}$$

where ΔT_1 the temperature difference of the hot and cold fluids on the inlet side, whereas the temperature difference on the outlet side is represented by ΔT_2.

$$\Delta T_1 = T_{h,in} - T_{c,out} \tag{3.16a}$$

$$\Delta T_2 = T_{h,out} - T_{c,in} \tag{3.16b}$$

The total heat transfer occurring in the heat exchanger is (Y. A. Cengel & Ghajar, 2020);

$$\dot{Q} = UA_s\Delta T_{lm} \tag{3.17}$$

where U is the overall heat transfer coefficient, A_s is the heat exchanger surface area, and ΔT_{lm} is the Logarithmic Mean Temperature Difference. The heat transfer performance of the heat exchanger is calculated by the heat transfer effectiveness of the heat exchanger (ε) (Y. A. Cengel & Ghajar, 2020);

$$\varepsilon = \frac{\dot{Q}_{act}}{\dot{Q}_{max}} = \frac{Actual\ heat\ transfer\ rate}{Maximum\ possible\ heat\ transfer\ rate} \quad (3.18)$$

where $\dot{Q}_{act}$ the actual amount of heat transferred from the hot or cold fluid;

$$\dot{Q}_{max} = C_{min}\Delta T_{max} \quad (3.19)$$

$$\Delta T_{max} = T_{h,in} - T_{c,in} \quad (3.20)$$

$\dot{Q}_{max}$ is the maximum heat transfer from the heat exchanger, C_{min} is the smaller of the two heat capacity rates, and ΔT_{max} indicates the highest temperature difference.

3.3. Numerical Study

For the numerical study, ANSYS 2022 R1 software was utilized due to its advanced capabilities and reliability in CFD simulations. The three-dimensional geometry was meticulously created using SpaceClaim, which provides a robust platform for geometric modeling. This geometry was then imported into Fluent Meshing, where the mesh structure was developed. To ensure high accuracy and resolution in the simulation, a combination of polyhedral (poly) and hexahedral (hex) mesh elements was employed. Poly mesh elements were chosen for their ability to conform to complex geometries, providing greater flexibility and precision in capturing the intricate details of the flow domain. Hex mesh elements were used to enhance the computational efficiency and stability of the simulation. The resulting mesh structure was rigorously tested to ensure it met the quality criteria required for an accurate and reliable simulation.

An outline view of the numerical model geometry, showcasing the detailed mesh structure and the overall configuration of the model, is presented in Figure 3.5. This visualization highlights the careful consideration given to the mesh design and the thorough preparation undertaken for the numerical analysis.

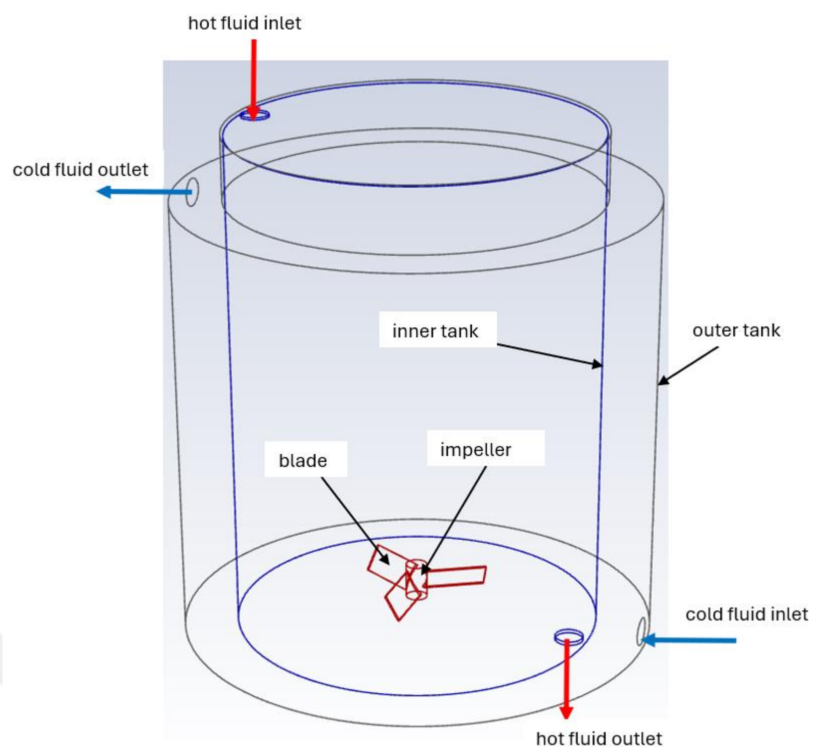

Figure 3.5. The 3D geometry and components of the numerical study

3.3.1. Verification of the Numerical Study

To verify the accuracy of the numerical study, it is essential to ensure that the numerical model achieves independence from both the mesh number and the number of iterations. This involves conducting a mesh independence study, where the results are checked for consistency across different mesh densities to ensure that further refinement does not significantly alter the outcome. Similarly, an iteration independence study is conducted to confirm that the solution converges and remains stable regardless of the number of iterations performed. Achieving this independence is crucial for verifying the reliability and robustness of the numerical model, ensuring that the results are accurate and not influenced by these computational parameters.

3.3.1.1. Mesh Independence Study

It is necessary for the created numerical model to be independent of its own mesh structure in order to demonstrate the accuracy of the study. In this context, five different mesh structures representing the numerical model have been created. In the numerical geometry, cells are concentrated at the solid-liquid interface to better resolve the effects in the thermal boundary layer and the hydrodynamic boundary layer. The coarsest mesh structure (Model 1) and the mesh structure (Model 4) generated for the numerical geometry are presented in Figure 3.6.

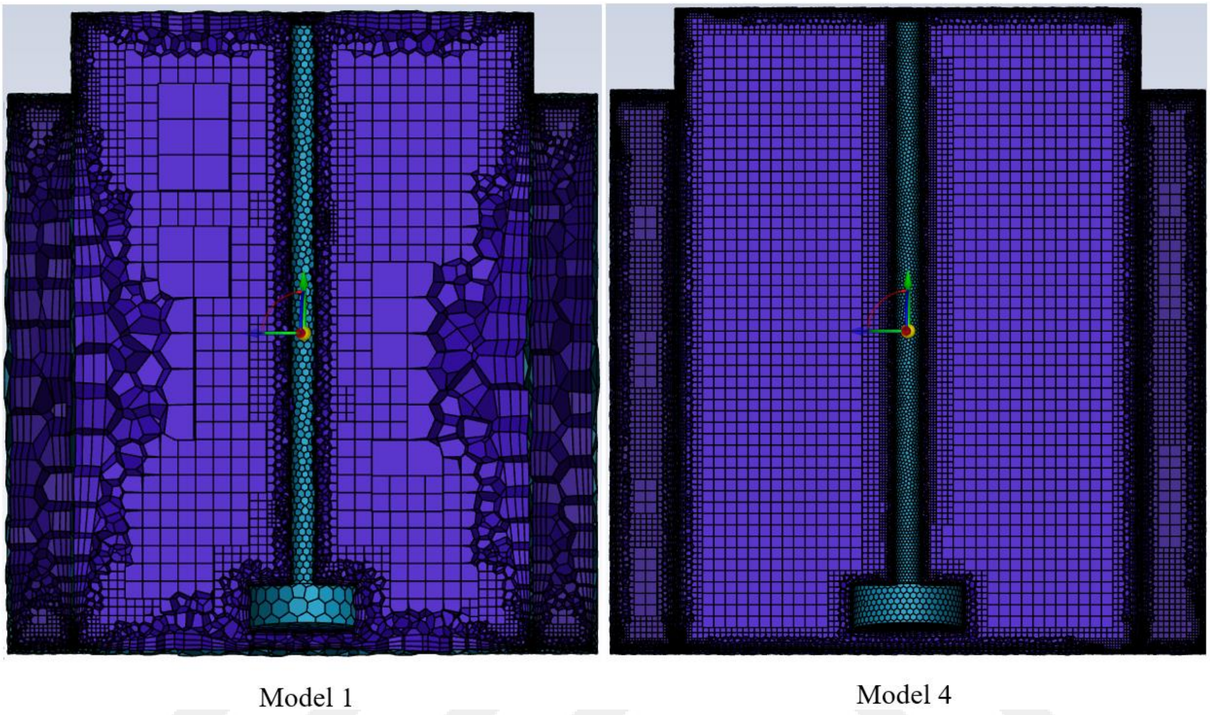

Figure 3.6. The coarsest mesh structure (Model 1) and the mesh structure used in the computational analysis (Model 4)

The difference in mesh structure between these two models is due to the number of elements. In the model with a higher number of elements, the program automatically selected hex mesh elements to achieve skewness and orthogonal quality values. The orthogonal quality values and skewness values for the models with five different mesh densities are presented in Table 2. This table provides a detailed comparison of the mesh quality metrics, which are crucial for ensuring the accuracy and reliability of the numerical simulations. Orthogonal quality is an indicator of the grid alignment with the flow field, with higher values signifying better alignment and less numerical error. Skewness measures the deviation of cell shapes from an ideal configuration, with lower values indicating better cell quality. By analyzing these metrics across different mesh densities, the table helps in identifying the optimal mesh configuration that balances computational efficiency and accuracy, ensuring robust and reliable simulation results.

Table 2. Different mesh structures and skewness values based on the number of cells.

Mesh structure	Cell number	Average skewness	Maximum skewness	Average orthogonal quality	Minimum orthogonal quality
Model 1	267491	0.263	0.83	0.794	0.21
Model 2	512361	0.141	0.78	0.867	0.27
Model 3	803545	0.123	0.68	0.881	0.32
Model 4	1279637	0.104	0.65	0.903	0.34
Model 5	1645901	0.102	0.63	0.912	0.35

The increase in the number of meshes has generally led to improved quality values, reflecting better grid alignment and reduced numerical errors. However, it was observed that beyond a mesh count of 1,200,000, the improvements in quality values became negligible. This indicates a point of diminishing returns where further increasing the mesh density does not significantly enhance the mesh quality. Additionally, a very high mesh count would considerably increase the computational time and resources required. Therefore, for this study, Model 4, with a mesh number of 1,279,637, was selected as the most suitable model.

To ensure mesh independence, a thorough test was conducted using the outlet temperature of the hot fluid in the heat exchanger as the key metric. This test is crucial for verifying that the simulation results are not significantly affected by the mesh density. By plotting the variation of the fluid outlet temperature against different mesh counts, the analysis determines if the solution has reached mesh independence. Figure 3.7. presents this variation, illustrating how the fluid outlet temperature changes with increasing mesh numbers. The results indicate that beyond a certain mesh count, the changes in outlet temperature become minimal, confirming that the chosen mesh density is sufficient for accurate and reliable simulation results without unnecessary computational expense.

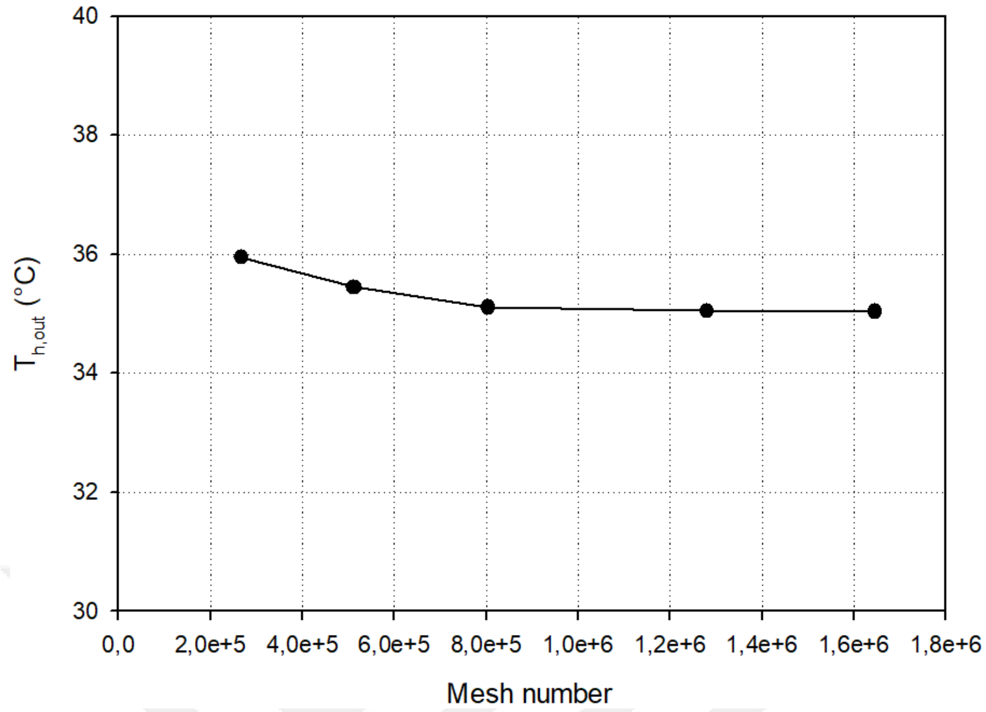

Figure 3.7. The variation of the hot fluid outlet temperature with respect to mesh number

3.3.1.2. Iteration Dependency Test

To achieve independence from the number of iterations, the solution was refined by setting the convergence criteria such that the energy residuals approached 10^{-6} while the momentum and turbulence residuals were adjusted to converge towards 10^{-3}. This approach ensures that the numerical solution is stable and accurate, minimizing numerical errors and providing reliable results. The stringent convergence criteria for energy residuals ensure precise thermal analysis, while the criteria for momentum and turbulence residuals allow for accurate prediction of flow and turbulence characteristics within the system. It was observed that after 500 iterations, there was no significant reduction in error values, indicating convergence. Consequently, to avoid unnecessarily prolonging the computation time, the numerical analyses were finalized using 500 iterations. This approach balances the need for accuracy with computational efficiency, ensuring reliable results without excessive use of resources. Figure 3.8. illustrates the convergence of the continuity, momentum, energy, and turbulence curves.

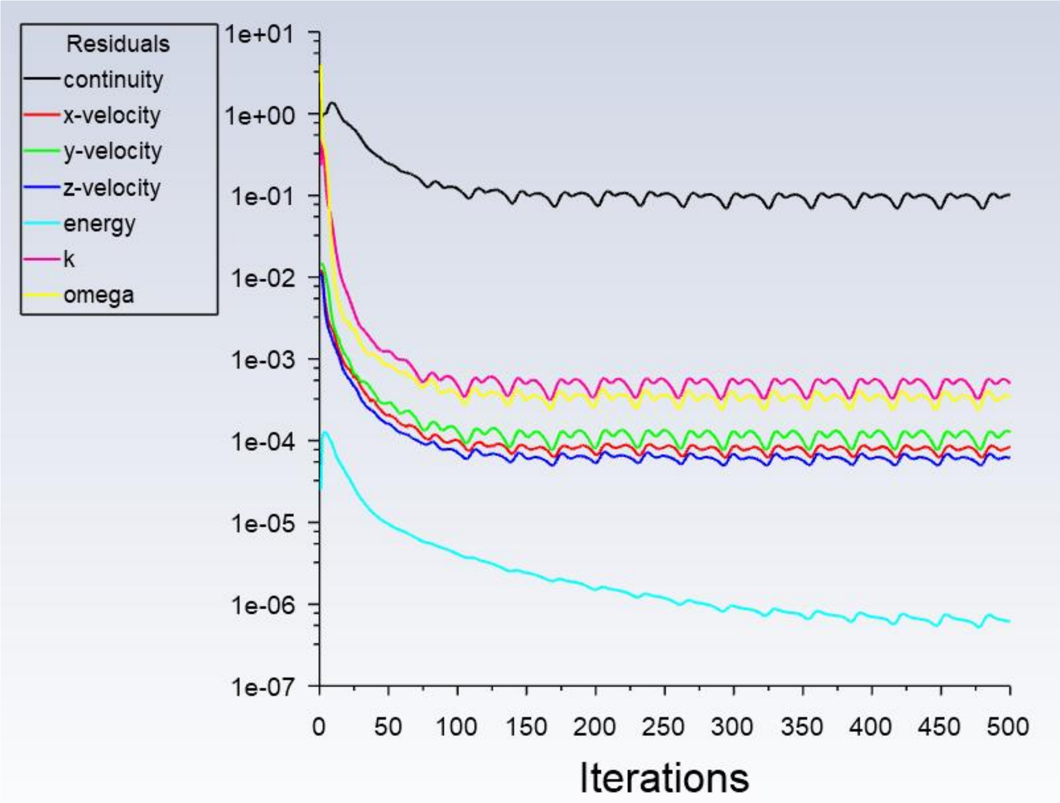

Figure 3.8. The convergence of the continuity, momentum, energy, and turbulence curves

Figure 3.9. shows the effect of this solution's convergence on the hot fluid outlet temperature. This figure demonstrates how the outlet temperature stabilizes as the solution converges, further validating the accuracy and stability of the numerical analysis.

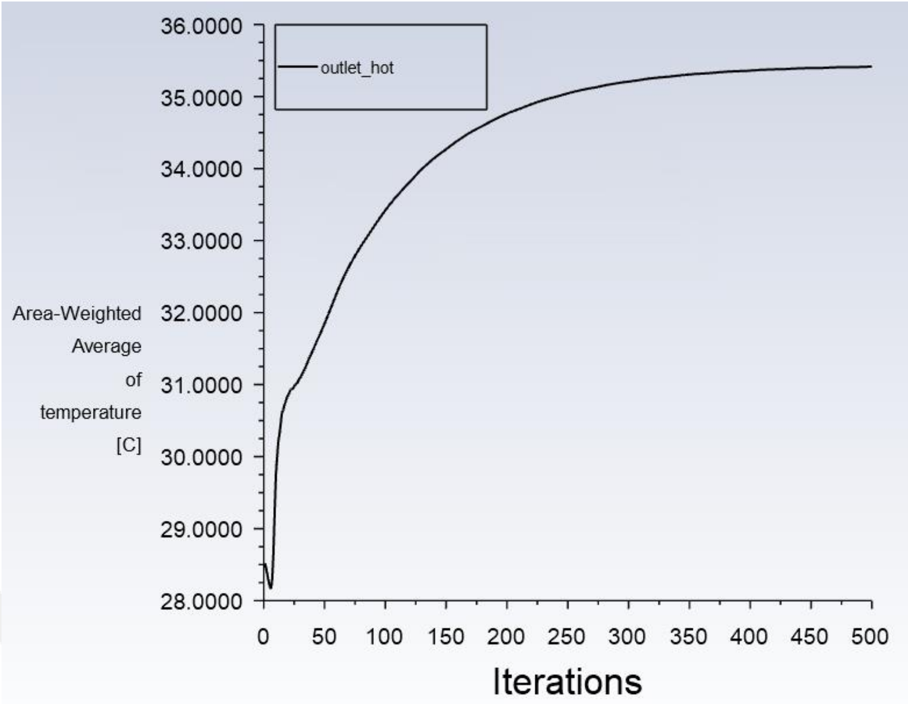

Figure 3.9. The convergence of the study depending on the hot fluid outlet temperature

3.3.2. Boundary Conditions

The boundary conditions for this thesis study are defined within a cylindrical coordinate system, which is suitable for the geometry and flow characteristics of the heat exchanger being analyzed. In this coordinate system, the velocity components are expressed as U_r (radial direction), U_θ (tangential or circumferential direction), and U_z (axial direction). For the hot and cold fluid inlets, radial and axial velocities are zero, with specified radial and tangential velocities and temperatures. At the outlets, velocity and temperature gradients are zero, indicating fully developed flow. The tank and stirrer have no-slip conditions with specified tangential velocities for the stirrer and adiabatic conditions, ensuring accurate simulation of fluid dynamics and heat transfer. The boundary conditions for the problem are presented in Table 3.

Table 3. The boundary conditions for the problem

Boundaries	**U_r (m/s)**	**U_θ (m/s)**	**U_z (m/s)**	**T (K)**	**P (Pa)**	**k (m^2/s^2)**	**ω (1/s)**
Hot fluid inlet	U_r=0	U_θ= V_{in}	U_z=0	T=$T_{h,in}$	P=$P_{h,in}$	k=k_{in}	ω=ω_{in}

Cold fluid inlet	$U_r = U_{in}$	$U_\theta = 0$	$U_z = 0$	$T = T_{c,in}$	$P = P_{c,in}$	$k = k_{in}$	$\omega = \omega_{in}$
Hot fluid outlet	$\frac{\partial U_r}{\partial y} = 0$	$\frac{\partial U_\theta}{\partial y} = 0$	$\frac{\partial U_z}{\partial y} = 0$	$\frac{\partial T}{\partial y} = 0$	$\frac{\partial P}{\partial y} = 0$	$\frac{\partial k}{\partial y} = 0$	$\frac{\partial \omega}{\partial y} = 0$
Cold fluid outlet	$\frac{\partial U_r}{\partial x} = 0$	$\frac{\partial U_\theta}{\partial x} = 0$	$\frac{\partial U_z}{\partial x} = 0$	$\frac{\partial T}{\partial x} = 0$	$\frac{\partial P}{\partial x} = 0$	$\frac{\partial k}{\partial x} = 0$	$\frac{\partial \omega}{\partial x} = 0$
Tank	$U_r = 0$	$U_\theta = 0$	$U_z = 0$	$\frac{\partial T}{\partial z} = 0$	$\frac{\partial P}{\partial z} = 0$	$k = 0$	$\omega = 0$
Impeller	$U_r = 0$	$U_\theta = V_{imp}$	$U_z = 0$	$\frac{\partial T}{\partial z} = 0$	$\frac{\partial P}{\partial z} = 0$	$\frac{\partial k}{\partial z} = 0$	$\frac{\partial \omega}{\partial z} = 0$

3.3.3. Validation of the Numerical Study

In order to validate the numerical model representing the experimental study, five different turbulence models were initially compared with the experimental results. At a constant Reynolds number (Re_{hot}=6000, Re_{cold}=2600) and constant fluid inlet temperatures (T_{hot}=40°C, T_{cold}=17°C), the stirrer rotational velocity was gradually increased from 0 to 300 rpm, and the numerical model's analysis results were compared with the experimental data. The comparison revealed that the SST k-omega model with low Reynolds correction best represented the experimental data with. It was modeled accurately, with a maximum error of 11%, showing good agreement with the experimental results. The comparison of experimental results with different turbulence models according to rotational velocity of the stirrer on heat transfer effectiveness is presented in Figure 3.10.

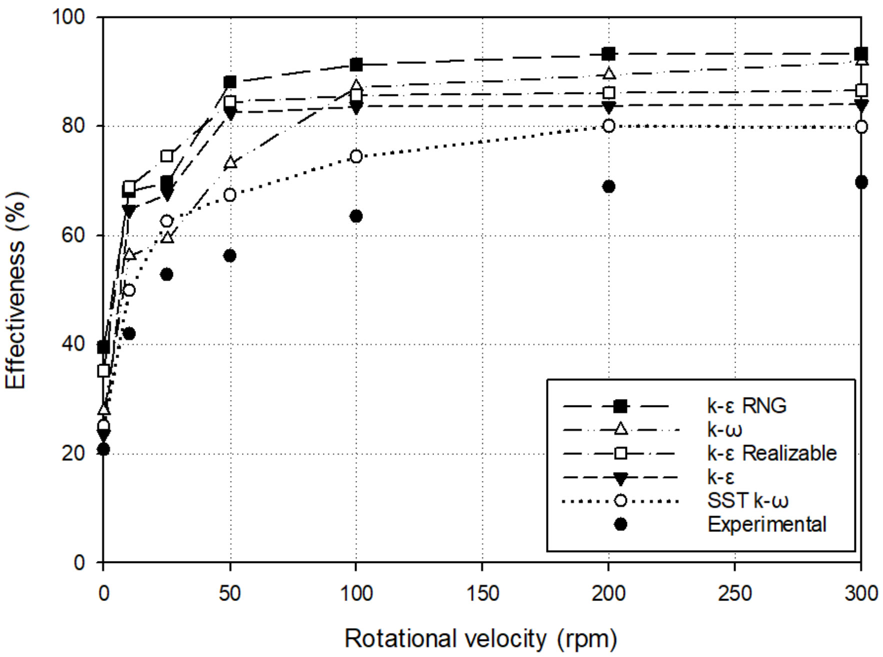

Figure 3.10. The comparison of experimental results with different turbulence models

Additionally, after deciding the turbulence model, a comparison of this model with the experimental study was conducted based on the Reynolds number. The comparison of heat transfer effectiveness depending on Reynolds number for the experimental study, both with the stirrer not rotating and rotating at 100 rpm, is presented in Figure 3.11. When the stirrer was not rotating, and the Reynolds number was increased within the range of 4000 to 10000, the maximum error observed was 8%. In contrast, when the stirrer was rotating at 100 rpm, the maximum error identified was 10%. These results indicate that the numerical model maintains a high level of accuracy under varying flow conditions, with acceptable deviations from the experimental data.

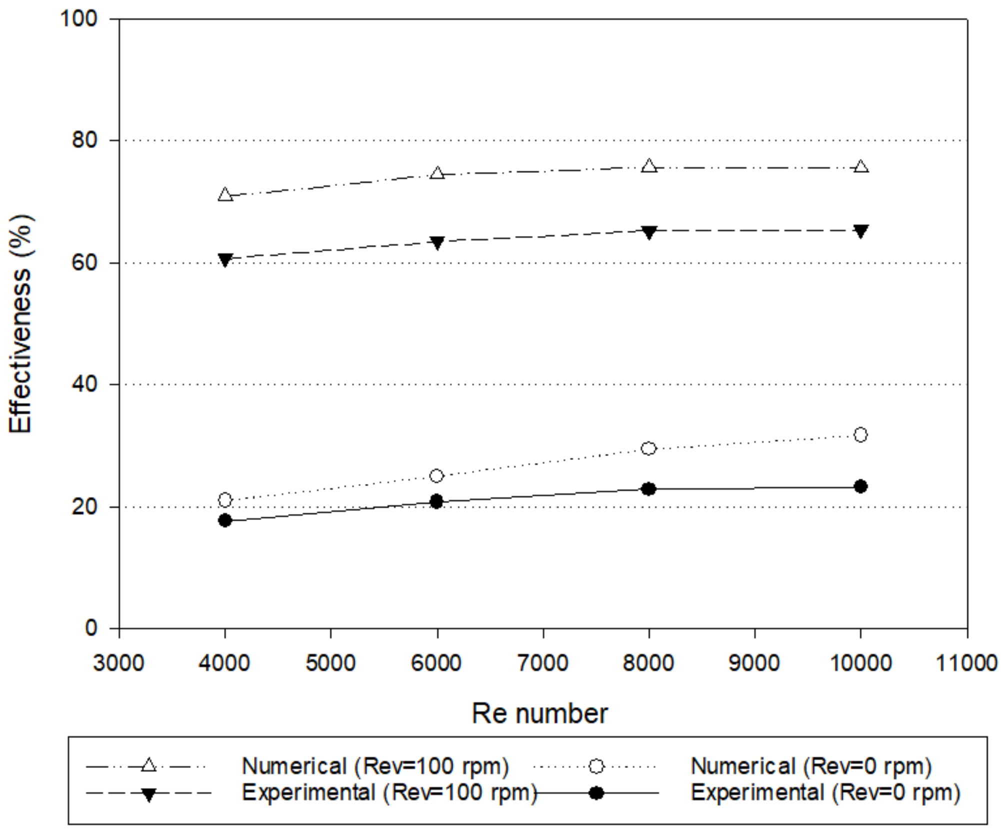

Figure 3.11. Heat transfer effectiveness based on Reynolds number

4. RESULTS AND DISCUSSION

In this section, the study results are examined in two stages. In the first stage, the results of the experimental work are analyzed. In the second stage, the developed numerical model is evaluated, and the heat transfer performance is assessed for each parameter determined in the study, providing an overall evaluation.

4.1. Experimental Results

The effects of Reynolds number, hot fluid inlet temperature, and rotational velocity of mechanical stirrer on heat transfer effectiveness in a stirred heat exchanger were experimentally investigated. In the heat exchanger, pure water has been used both as the cold and hot fluid. The fluid flow has been configured as counter flow. The parameters investigated in the experimental study presented in Table 4.

Table 4. The parameters studied in the experimental setup

Groups	Constant variables	Parameters	Number of experiments
1	$T_{c,in}$=17°C $T_{h,in}$=40°C Rev=100 rpm	Re=4000 Re=6000 Re=8000 Re=10000	3
2	$T_{c,in}$=17°C $T_{h,in}$=40°C Re=6000	Rev=0 rpm Rev=100 rpm Rev=200 rpm Rev=300 rpm	3
3	$T_{c,in}$=17°C Re=6000 Rev=100 rpm	$T_{h,in}$=30°C $T_{h,in}$=40°C $T_{h,in}$=50°C $T_{h,in}$=55°C	3

4.1.1. The Effect of Reynolds Number on Heat Transfer Performance

To determine the effect of Reynolds number on heat transfer effectiveness, the results were investigated under two conditions: one where the mechanical stirrer was stationary and another where it rotated at 100 rpm. When the inlet temperature of the hot fluid $T_{h,in}$=40°C and cold fluid $T_{c,in}$=17 was constant and rotational velocity of the stirrer was 0 rpm, the Reynolds number

(Re) was increased gradually in the range of 4000-10000. When Re number was increased in the range of 4000-6000 there was a 3.1% increase in heat transfer effectiveness; when Re number was increased in the range of 6000-8000, there was a 2.1% increase; and when Re number was increased in the range of 8000-10000, 0.4% increase was observed. Overall, 5.6% increase in heat transfer effectiveness was observed when the Reynolds number was increased in the range of 4000-10000. The effect of Reynolds number on heat transfer effectiveness for 0, 100, 200 and 300 rpm are presented in Figure 4.1.

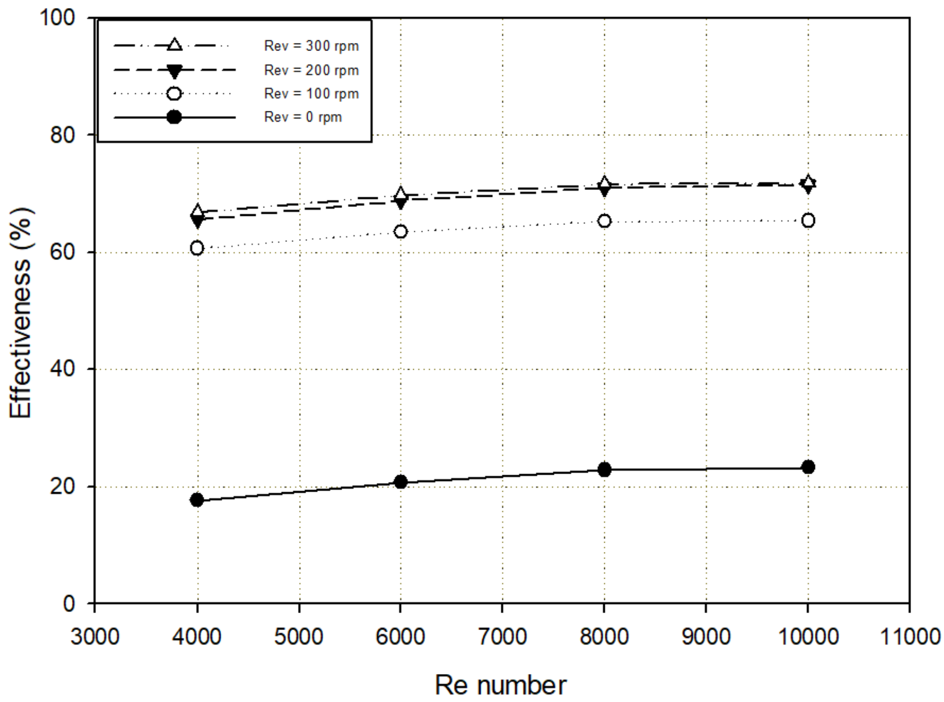

Figure 4.1. The effect of Reynolds number on heat transfer effectiveness

For the same boundary conditions, the effect of the Reynolds number on heat transfer performance was investigated while the mechanical stirrer speed was set to 100 rpm. When Re number was increased in the range of 4000-6000 there was a 2.8% increase in heat transfer effectiveness; when Re number was increased in the range of 6000-8000, there was a 1.8% increase; and when Re number was increased in the range of 8000-10000, 0.1% increase was observed. Overall, 4.7% increase in heat transfer effectiveness was observed when the Reynolds number was increased in the range of 4000-10000.

4.1.2. The Effect of Rotational Velocity of the Stirrer on Heat Transfer Performance

In order to evaluate the effect of the mechanical stirrer's rotational velocity on heat transfer performance, the velocity was gradually increased in steps within the range of rpm=0-300 while the hot fluid inlet temperature was kept constant at 40°C and the hot fluid Reynolds number was maintained constant at Re=6000. When the rotational velocity was increased from 0 to 100 rpm, 42.7% increase in heat transfer effectiveness was observed. This effect was 5.4% in the range of 100-200 rpm and 0.9% in the range of 200-300 rpm. A total increase of 49% in heat transfer effectiveness was observed when the stirrer speed was increased in the range of Rev=0-300 rpm. The effect of rotational velocity of the stirrer on heat transfer effectiveness for different inlet temperatures is presented in Figure 4.2.

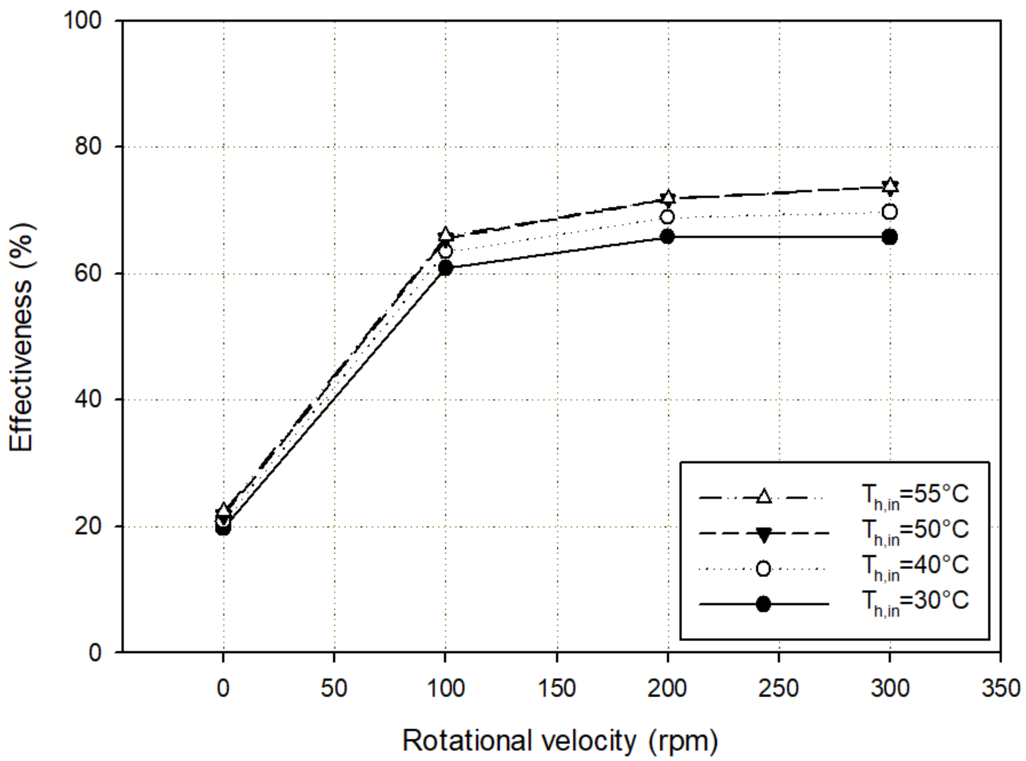

Figure 4.2. The effect of rotational velocity of the stirrer

4.1.3. The Effect of Inlet Temperature on Heat Transfer Performance

To investigate the effect of the hot fluid inlet temperature on heat transfer performance, the inlet temperature of the hot fluid was gradually increased within the range of 30-55°C for different rotation velocities at a Reynolds number of Re=6000. For the velocity of 100 rpm, increasing the temperature in the range of 30-40℃ has led to increase of 2.6%; in the range of 40-50℃ has led to increase of 2.1% and in the range of 50-55℃ has led to increase of 0.3% in heat transfer effectiveness. In the heat exchanger, a total increase of 5% in heat transfer effectiveness was observed when the hot fluid inlet temperature was increased in the range of 30-55℃. The effect of the increasing inlet temperature of the hot fluid on heat transfer effectiveness is presented in Figure 4.3.

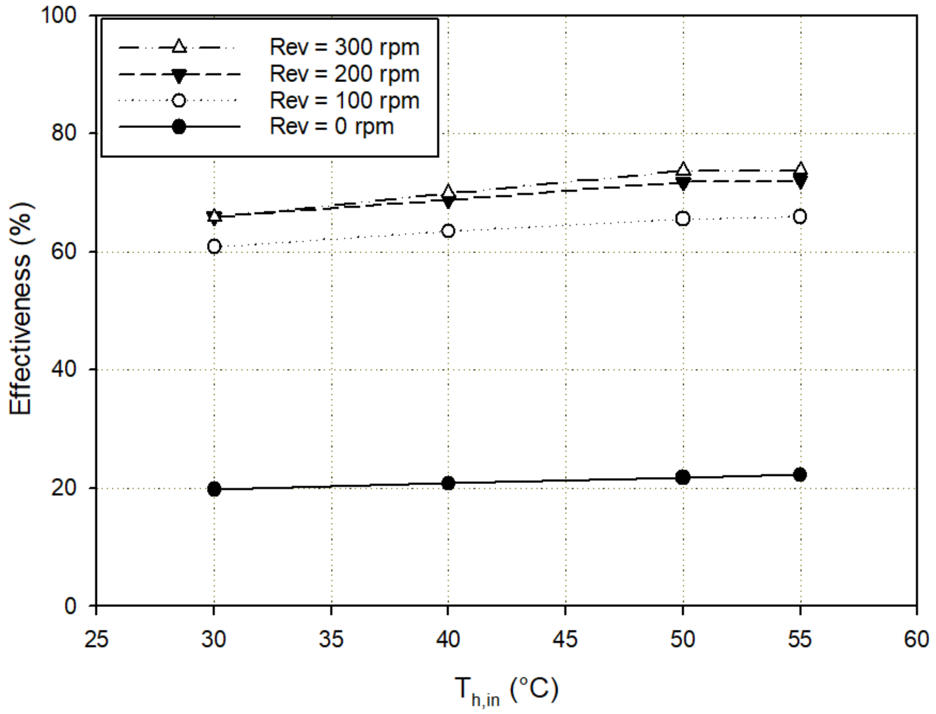

Figure 4.3. The effect of the increasing inlet temperature of the hot fluid

4.2. Numerical Results

For the numerical study, ANSYS 2022 R1 was used for its advanced CFD capabilities. The 3D geometry was created in SpaceClaim and meshed in Fluent Meshing with polyhedral and hexahedral elements to ensure high accuracy and resolution. The mesh structure was rigorously tested to meet quality criteria for reliable simulation. The SST k-ω turbulence model with low Re correction was found to model the study most accurately.

To accurately model the rotational motion of the mechanical stirrer and the resulting fluid dynamics, a moving reference frame (MRF) was defined. This approach allows for the simulation of the stirrer's rotational movement and its impact on the surrounding fluid within the computational domain, providing a more precise representation of the flow characteristics and interactions between the stirrer and the fluid (Patil et al., 2021). The MRF technique ensures that the rotational effects are captured effectively, facilitating a detailed analysis of the system's performance under different operational conditions. The problem was solved in a steady-state condition. The results obtained for each parameter in the numerical study were evaluated. In the generated numerical model, the flow properties for the cold fluid were set to $T_{c,in}$=17°C and Re = 2600; for the hot fluid, the flow properties were set to $T_{h,in}$=40°C and Re = 6000. The parameters for the numerical study are presented in Table 5.

Table 5. The parameters studied in the numerical study

Groups	Constant variables	Parameters	Description
1	D=40 mm H=10 mm θ=30° n=3 S=1	Rev=0 rpm Rev=10 rpm Rev=25 rpm Rev=50 rpm Rev=100 rpm Rev=200 rpm Rev=300 rpm Rev=400 rpm	Rotational velocity of mechanical stirrer
2	Rev=100 rpm D=40 mm θ=30° n=3 S=1	H=10 mm H=40 mm H=70 mm H=100 mm	Height of impeller hub from the bottom of the tank
3	Rev=100 rpm H=10 mm θ=30° n=3 S=1	D=40 mm D=60 mm D=80 mm D=100 mm	Outer diameter of the impeller
4	Rev=100 rpm D=40 mm H=10 mm n=3 S=1	θ=0° θ=15° θ=30° θ=45°	Angle to normal of the impeller blade
5	Rev=100 rpm D=40 mm H=10 mm θ=30°	n=2 n=3 n=5 n=7	Number of impeller blades which are around centerline

	S=1		
6	Rev=100 rpm D=40 mm H=10 mm θ=30° n=3	S=1 S=2 S=3	Number of stirrers equally spaced

In this table, D represents the outer diameter of the impeller including the blades, H represents the distance of the impeller from the bottom of the tank, θ represents the angle that the blade makes with the vertical y-axis, n represents the number of blades, and S represents the number of stirrers or impellers.

4.2.1. The Effect of Rotational Speed on Heat Transfer Performance

The effect of rotational speed on heat transfer effectiveness was investigated for different rotational speed with constant impeller diameter of D=40 mm, height of impeller H=10 mm, impeller blade angle θ=30°, number of impeller blade n=3 and number of stirrer S=1. When the rotational speed of the impeller was increased in the range of 0-10 rpm, 25% increase in heat transfer effectiveness was determined. The heat transfer effectiveness increased by 12.7% in the range of 10-25 rpm, by 4.7% in the range of 25-50 rpm, by 7.1% in the range of 50-100 rpm, by 5.6% in the range of 100-200 rpm. When the rotational speed of the mechanical stirrer was increased above 200 rpm, there was no improvement in heat transfer performance, and a 0.2% decrease was observed in the range of 200-300 rpm. When the rotational speed was increased in the range of 300-400 rpm, no significant difference in heat transfer performance was determined. The effect of increasing rotational speed on heat transfer effectiveness is presented in Figure 4.4.

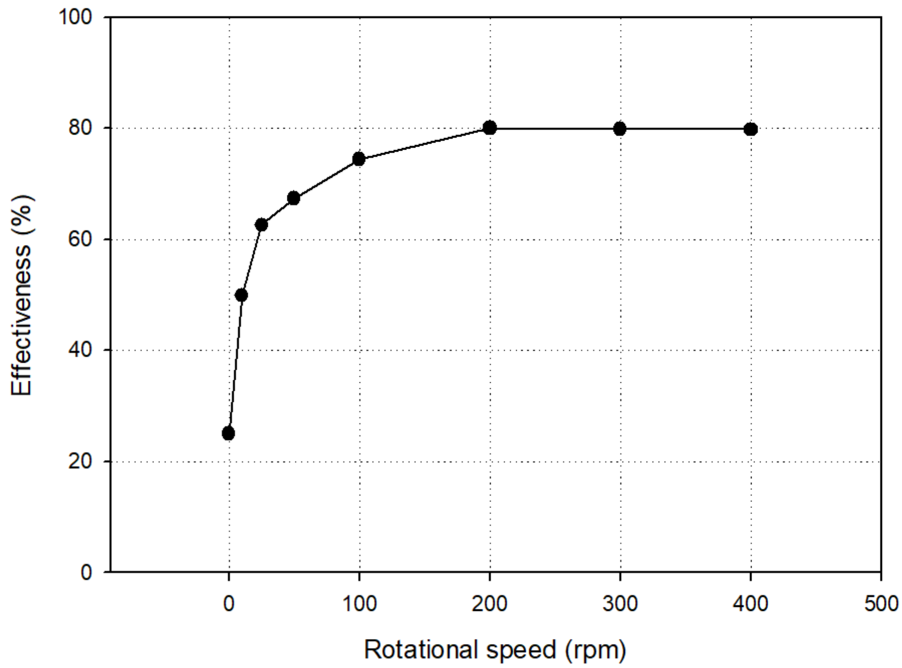

Figure 4.4. The effect of increasing rotational speed on heat transfer effectiveness

Overall, a total increase of 55.1% in heat transfer effectiveness was detected within the rotational velocity range of 0-200 rpm. The heat transfer performance in the heat exchanger shows a significant improvement when the impeller is rotating compared to when it is stationary. Although an increase in heat transfer performance is observed as the rotational speed increases, there is no significant change beyond 200 rpm. Temperature contours taken from an XZ plane passing through the center of the impeller for the range of Rev=0-400 are presented in Figure 4.5., 4.6., 4.7., and 4.8.

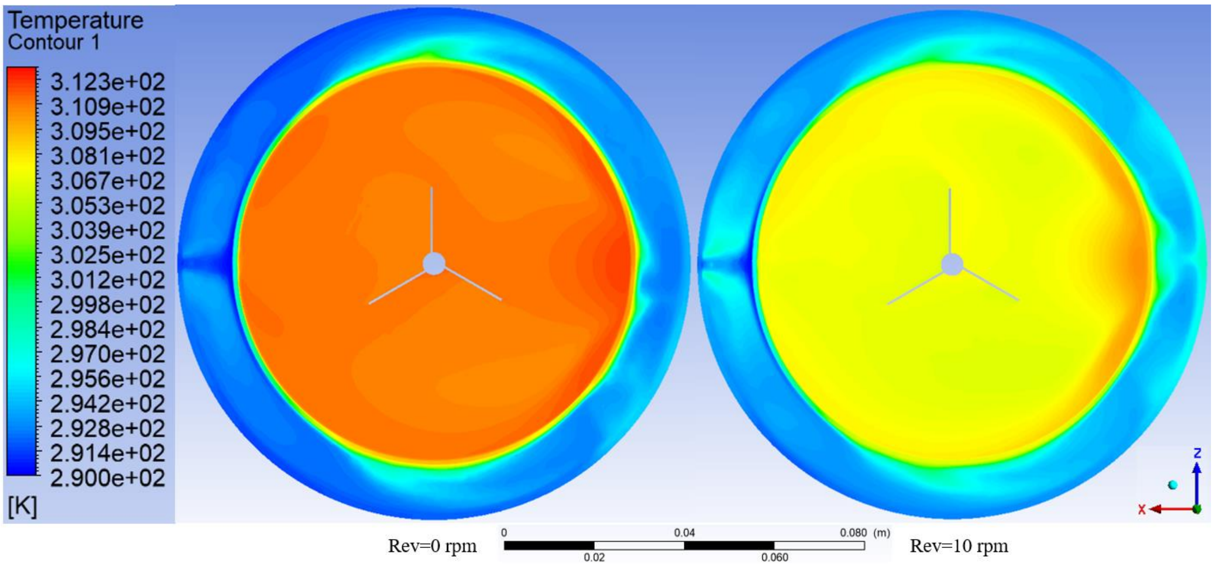

Figure 4.5. Temperature contours for Rev=0 rpm and Rev=10 rpm

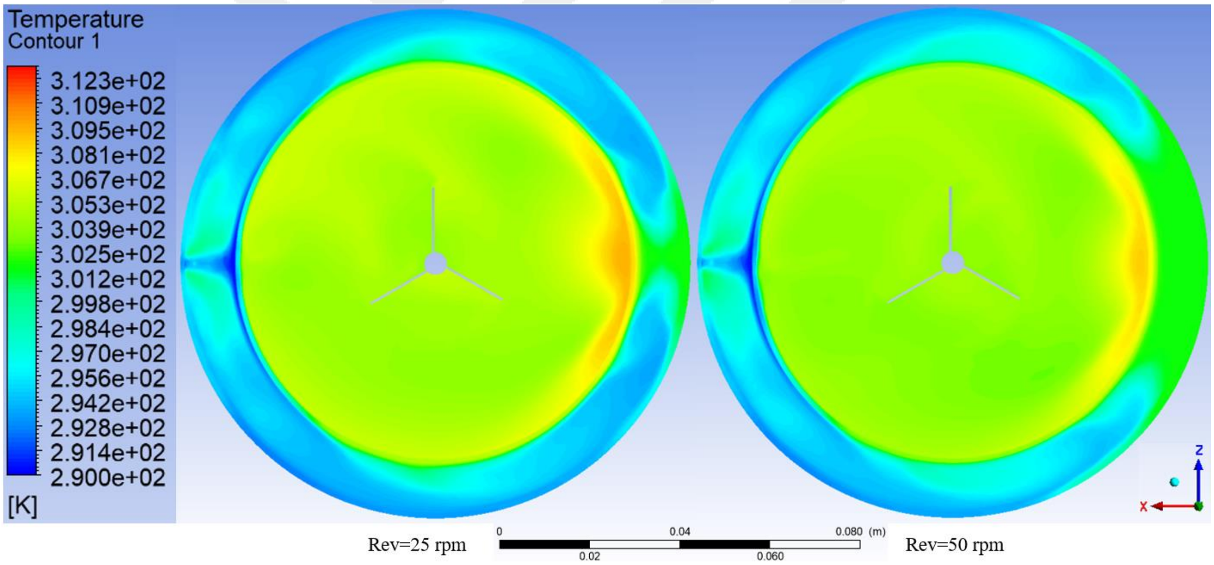

Figure 4.6. Temperature contours for Rev=25 rpm and Rev=50 rpm

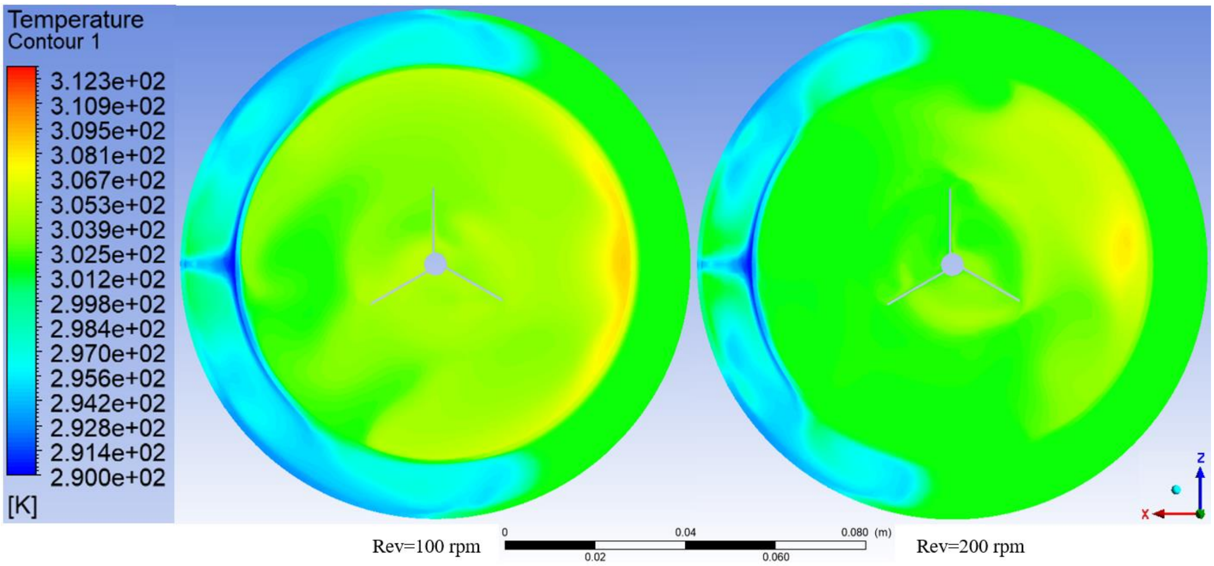

Figure 4.7. Temperature contours for Rev=100 rpm and Rev=200 rpm

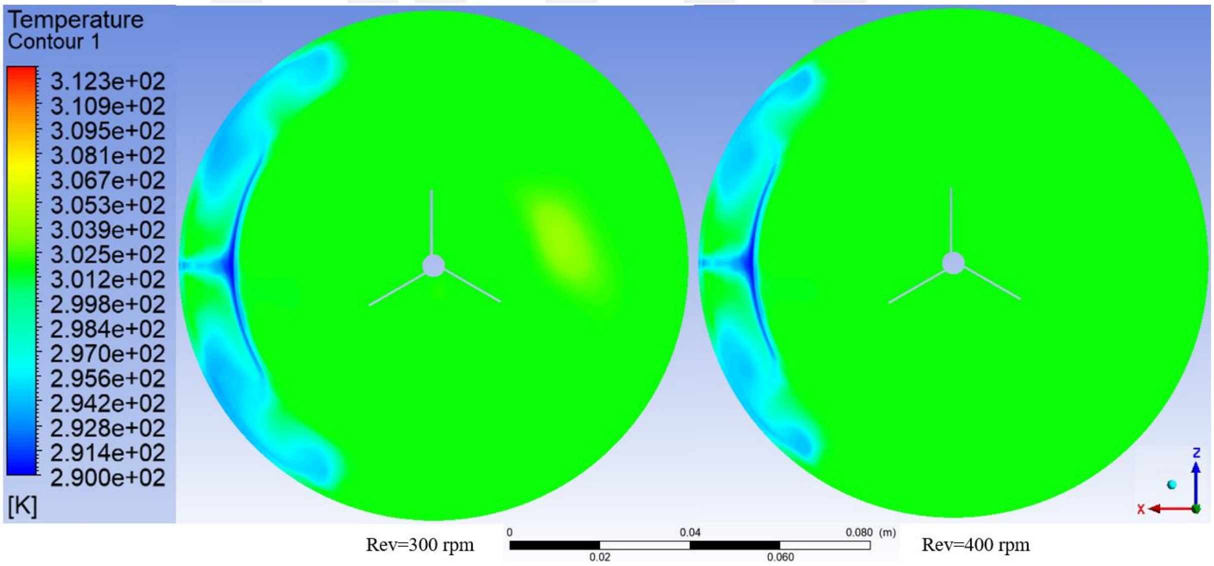

Figure 4.8. Temperature contours for Rev=300 rpm and Rev=400 rpm

Temperature contours taken from an XY plane created in the center of the impeller for the range of Rev=0-400 are presented in Figure 4.9., 4.10., 4.11., and 4.12.

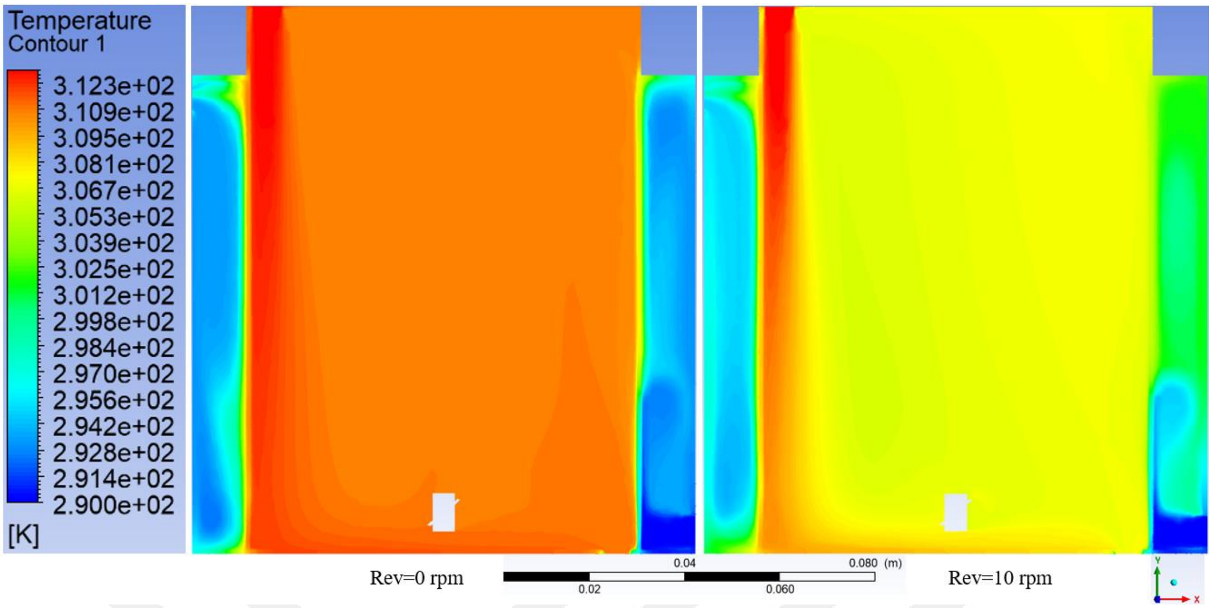

Figure 4.9. Temperature contours for Rev=0 rpm and Rev=10 rpm

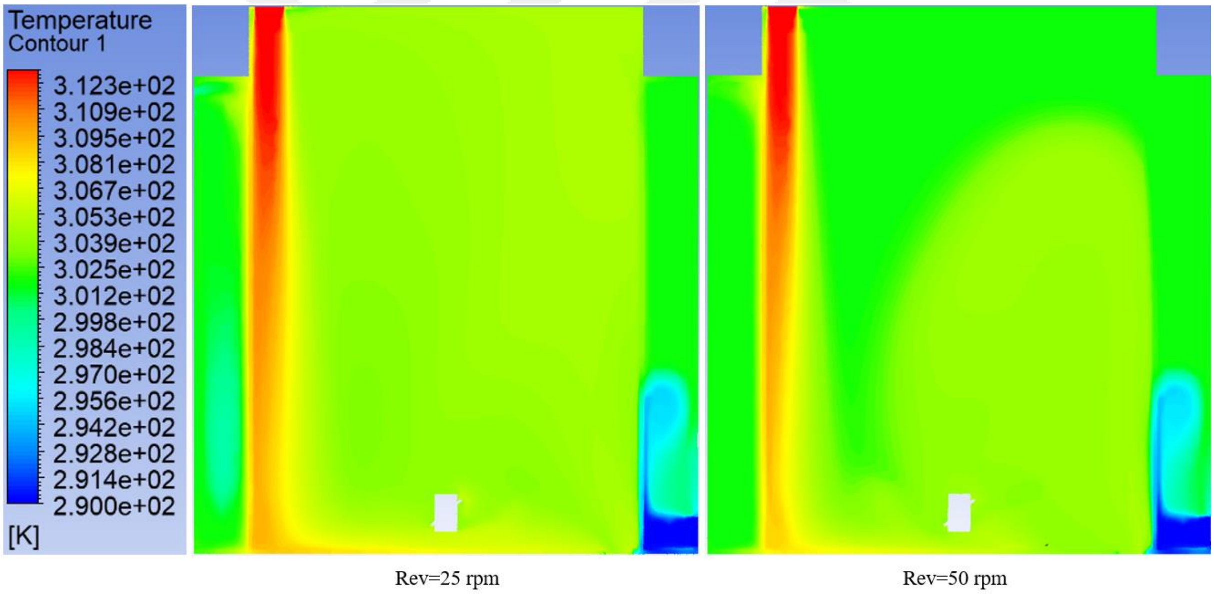

Figure 4.10. Temperature contours for Rev=25 rpm and Rev=50 rpm

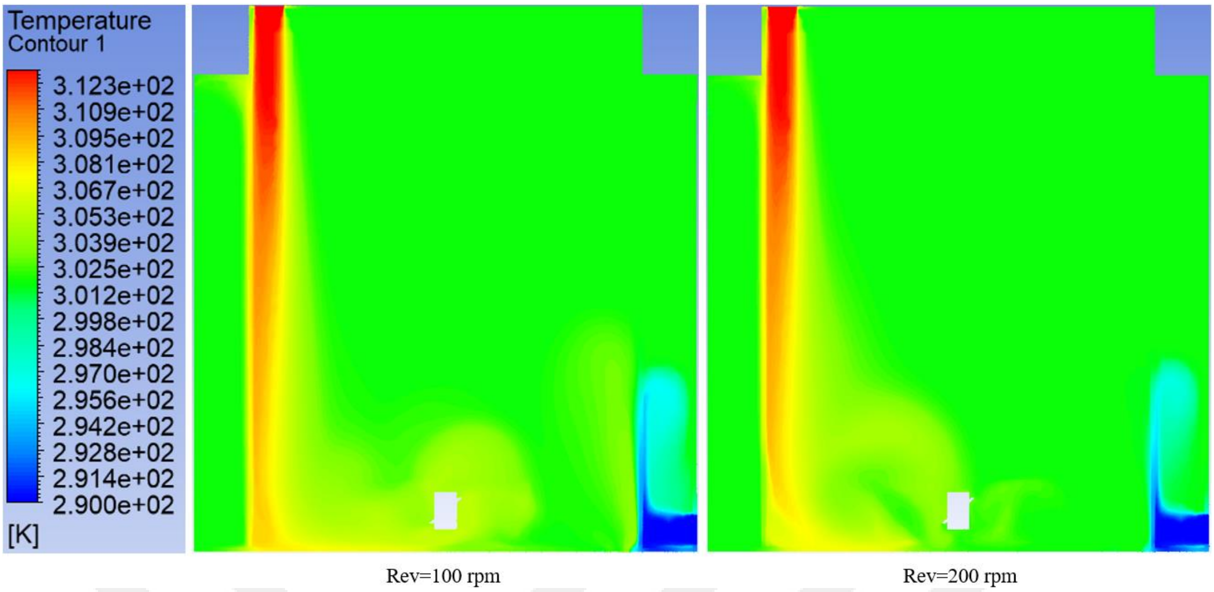

Figure 4.11. Temperature contours for Rev=100 rpm and Rev=200 rpm

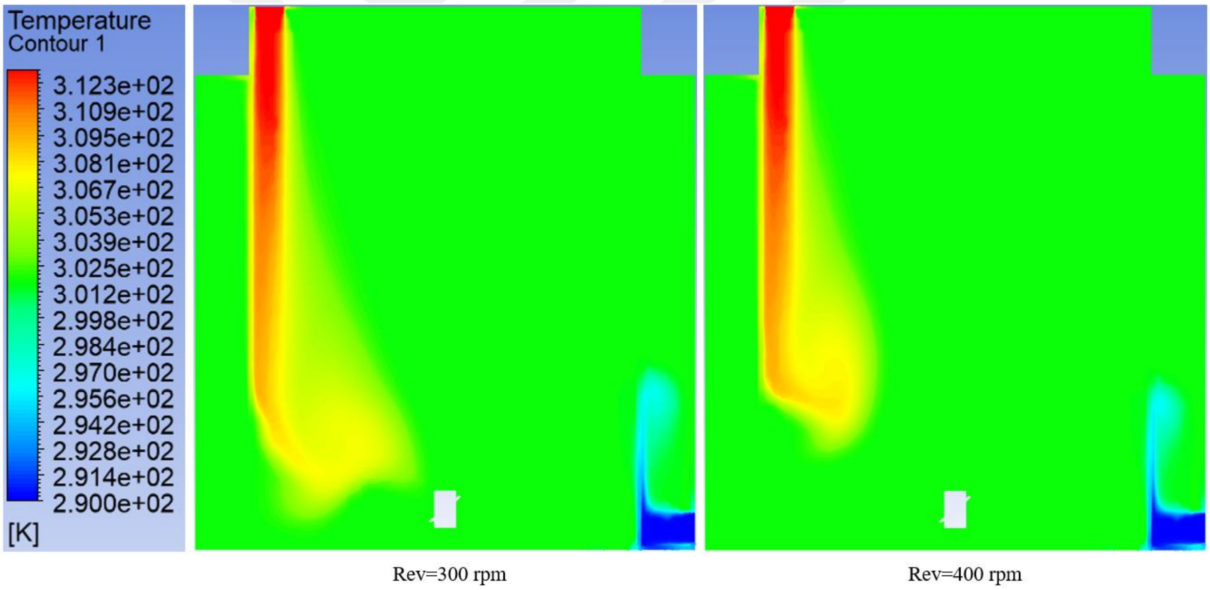

Figure 4.12. Temperature contours for Rev=300 rpm and Rev=400 rpm

Velocity vectors from the numerical analysis results are presented in Figure 4.13., 4.14., 4.15. and 4.16.

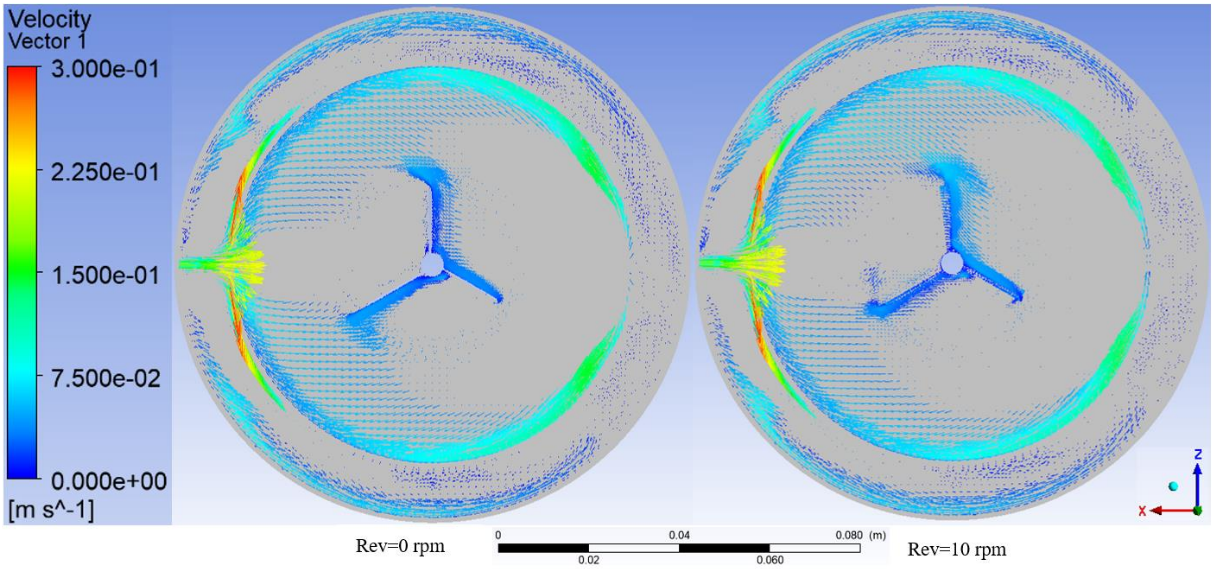

Figure 4.13. Velocity vectors for Rev=0 rpm and Rev=10 rpm

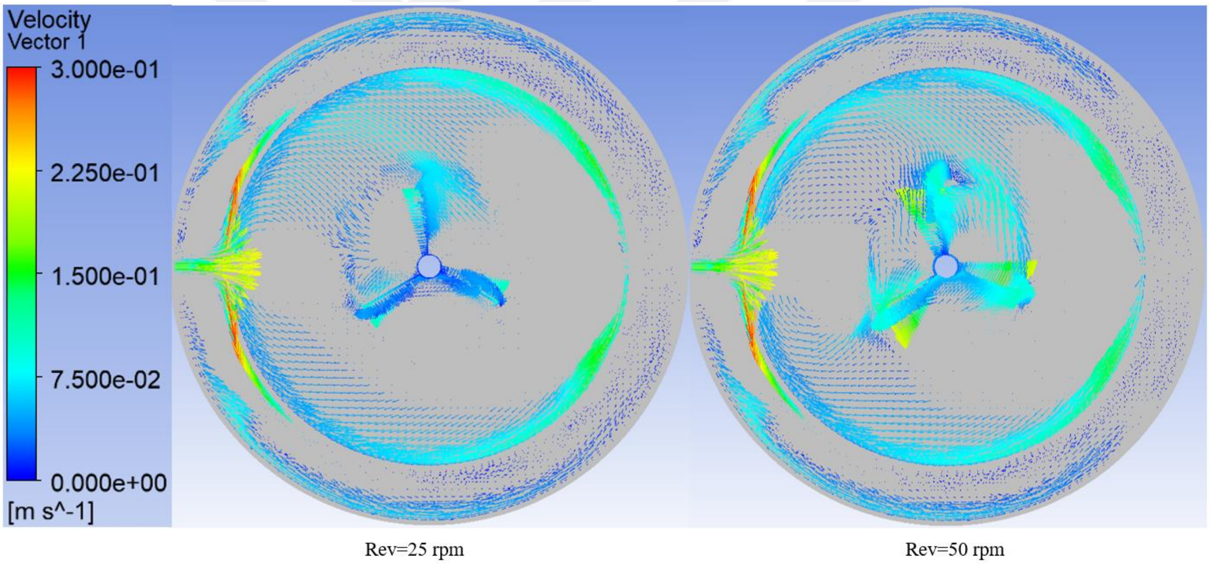

Figure 4.14. Velocity vectors for Rev=25 rpm and Rev=50 rpm

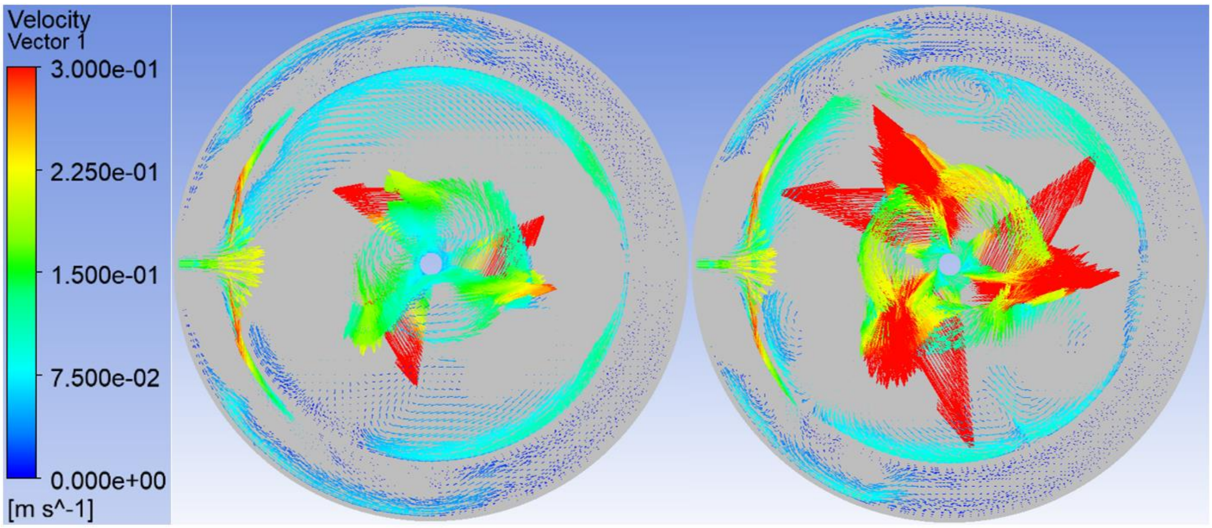

Rev=100 rpm Rev=200 rpm

Figure 4.15. Velocity vectors for Rev=100 rpm and Rev=200 rpm

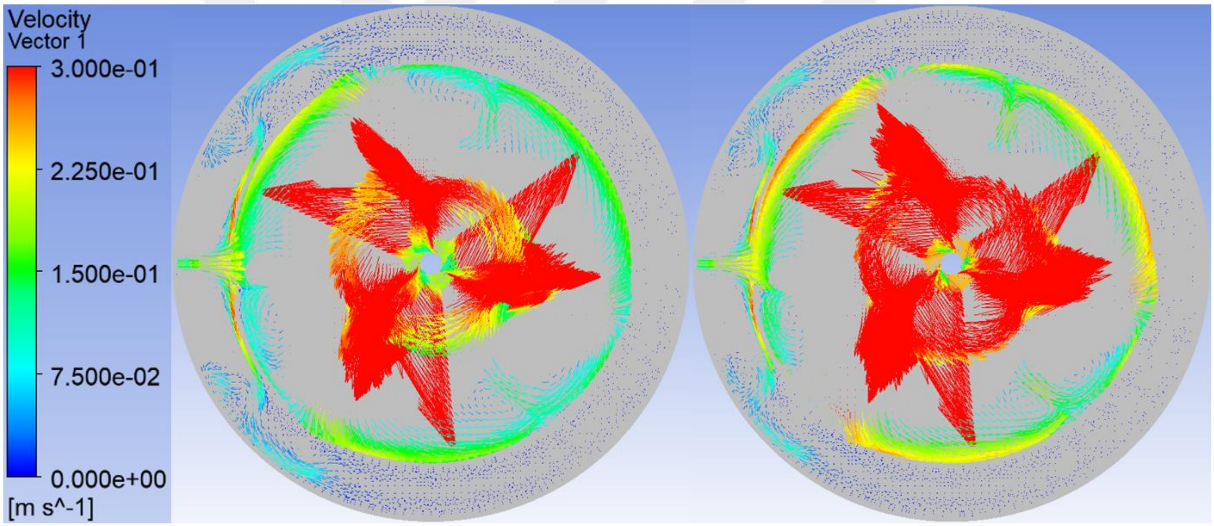

Rev=300 rpm Rev=400 rpm

Figure 4.16. Velocity vectors for Rev=300 rpm and Rev=400 rpm

4.2.2. The Effect of Height of the Impeller on Heat Transfer Performance

The effect of height of the impeller on heat transfer effectiveness was investigated for four different heights as H = 10, 40, 70, 100 mm. While all other variables remained constant, the 40 mm height from the bottom demonstrated 17.2% greater heat transfer performance than the height H=10 mm. Increasing the height of the mechanical stirrer from H = 40 mm to H = 70 mm caused a 0.94% decrease in heat transfer effectiveness. Increasing the height of the mechanical stirrer from H = 70 mm to H = 100 mm caused a 2.8% decrease in heat transfer effectiveness. The effect of the impeller's height from the bottom of the heat exchanger on heat transfer effectiveness is presented in Figure 4.17.

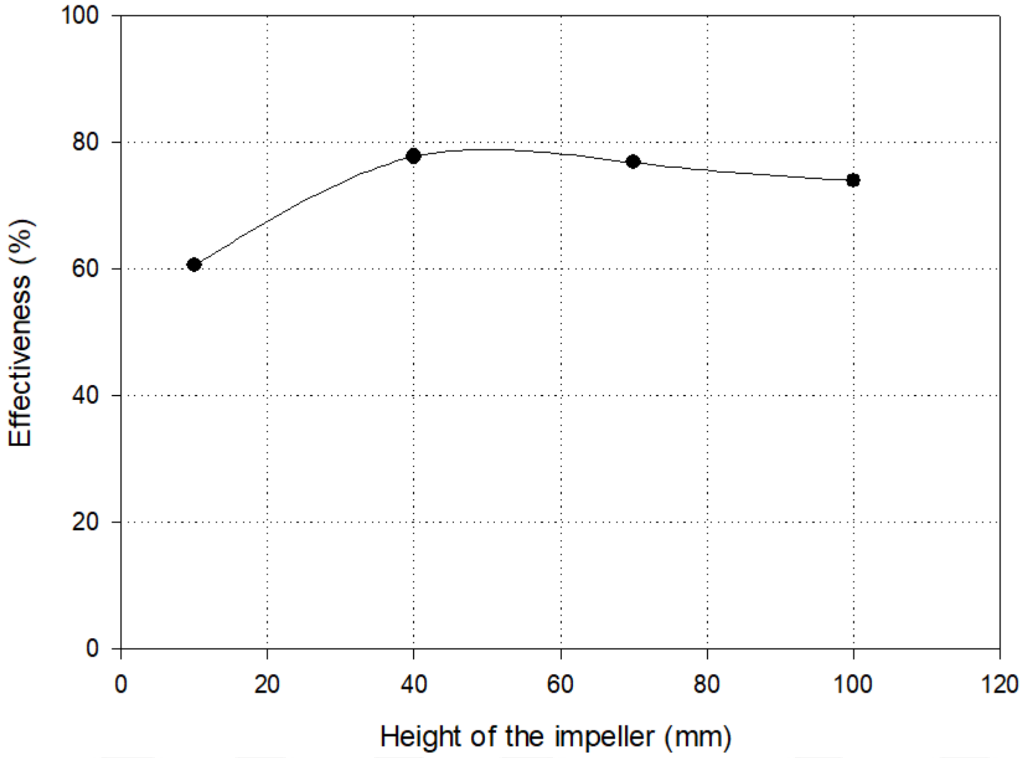

Figure 4.17. The effect of the impeller's height

The effect of the impeller’s height for H = 10 mm and H = 40 mm on heat transfer performance is illustrated by the temperature contours presented in Figure 4.18.

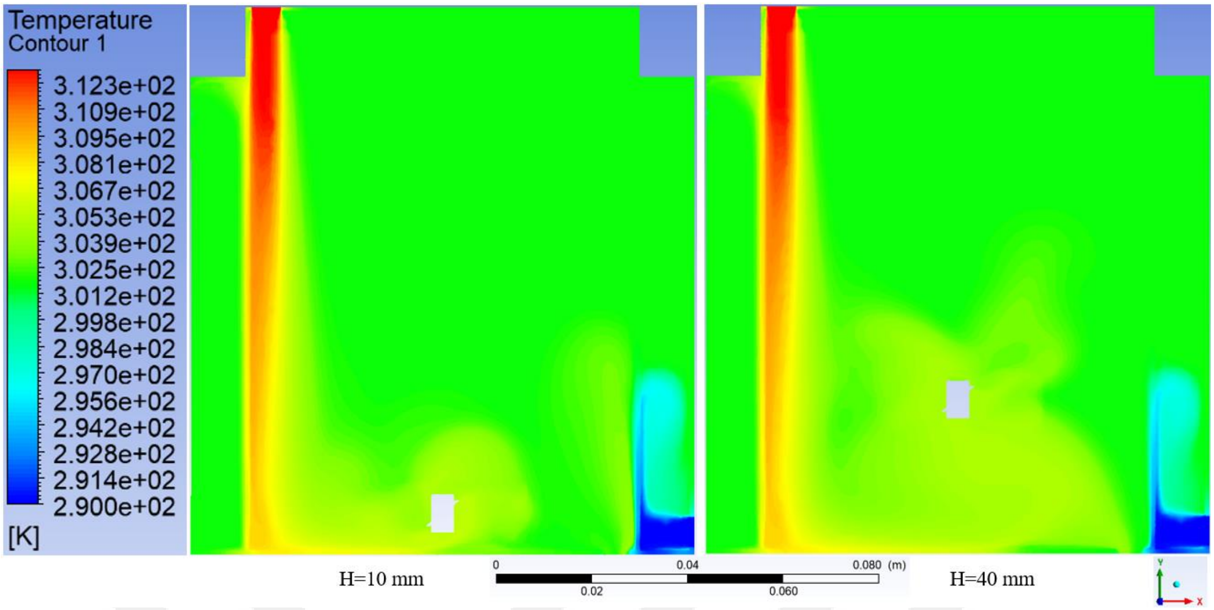

Figure 4.18. Temperature contours for H = 10 mm and H = 40 mm

It can be observed that when the impeller height is increased from 10 mm to 40 mm, the fluid mixing improves and the temperature distribution becomes more homogeneous, resulting in higher heat transfer performance.

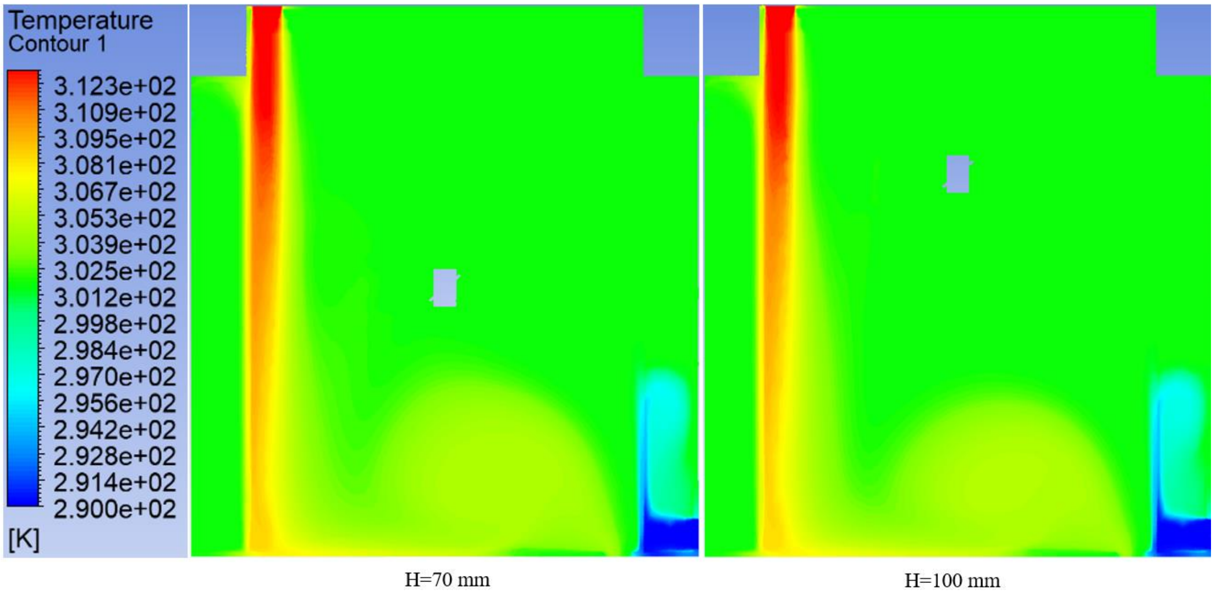

Figure 4.19. Temperature contours for H = 70 mm and H = 100 mm

It was observed in Figure 4.19. that when the impeller height was increased to 70 mm and 100 mm, there was no significant difference in the results. However, as the impeller height increased, a decrease in heat transfer effectiveness was detected. Velocity vectors in the XY plane created at the center of the impeller for four different impeller heights are presented in Figure 4.20 and 4.21.

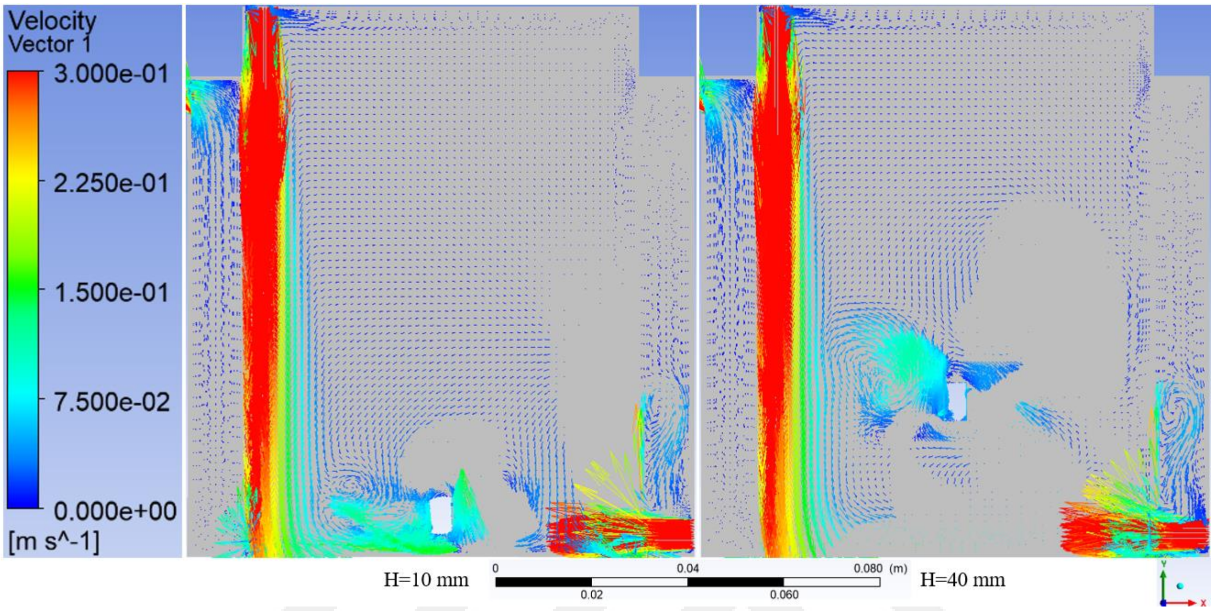

Figure 4.20. Velocity vectors for H = 10 mm and H = 40 mm

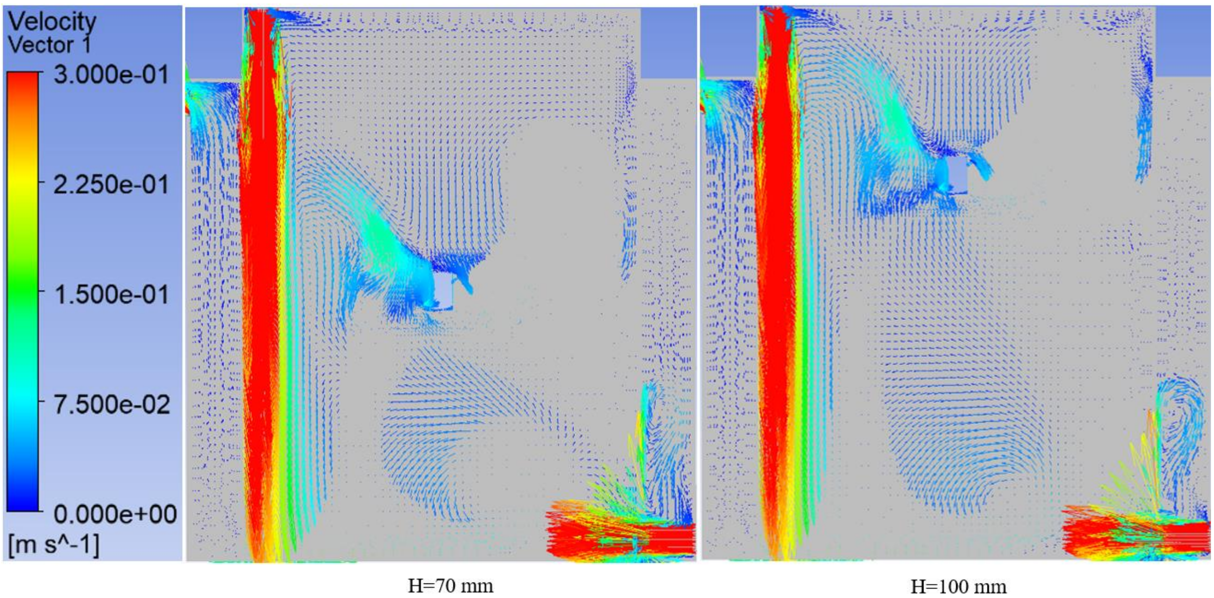

Figure 4.21. Velocity vectors for H = 70 mm and H = 100 mm

When examining the velocity vectors, it can be observed that for H = 40 mm, vortex formations increase, and high-velocity regions become more distinct in the upper part of the flow field.

4.2.3. The Effect of Diameter of the Impeller on Heat Transfer Performance

The effect of outer diameter of the impeller (D = 40, 60 80, 100 mm) on heat transfer performance was investigated, while angular velocity of 100 rpm, height of the impeller H = 10 mm, angle θ = 30°, number of blade n = 3 and number of stirrer S = 1 are constants. Increasing the diameter from 40 to 60 mm has led to increase in heat transfer effectiveness by 11.8%, from 60 to 80 mm has led to increase by 0.4%, from 80 to 100 mm has led to increase by 3.75%. As the impeller diameter increased, the improvement in heat transfer performance continued. Increase in diameter from 40 to 100 resulted in an overall increase of 15.9% in heat transfer effectiveness. The effect of the impeller diameter on heat transfer effectiveness is illustrated in the graph in Figure 4.22.

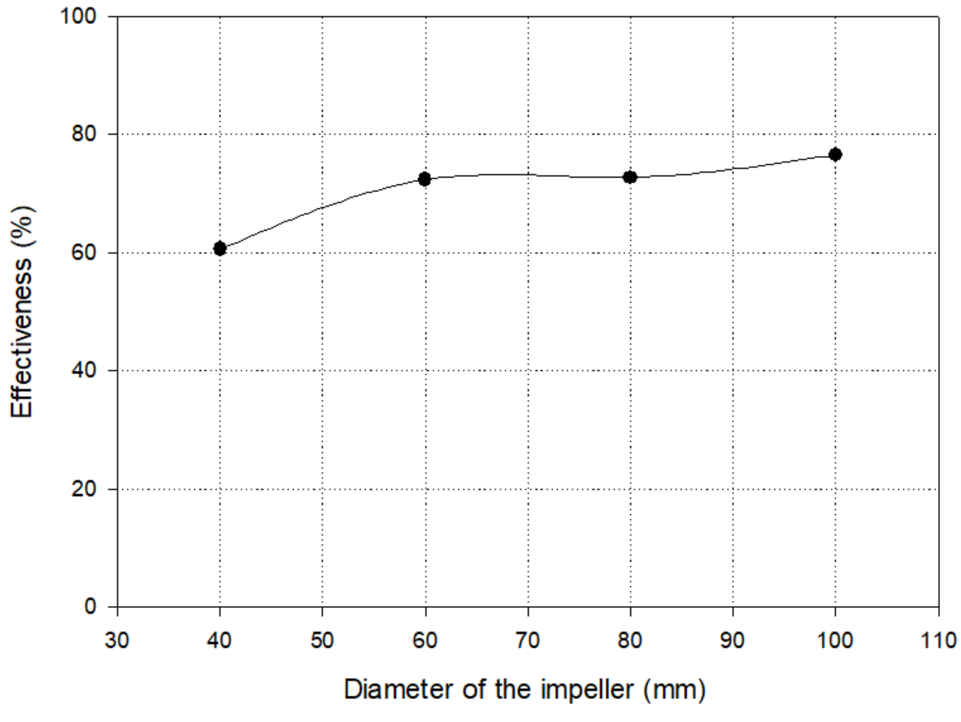

Figure 4.22. The effect of the impeller diameter on heat transfer effectiveness

While an increase in effectiveness is observed as the impeller diameter increases from 40 mm to 60 mm, no increase in effectiveness is detected between 60 mm and 80 mm. Up to this point, an optimum has been reached due to the mixing effect caused by fluid dynamics. However, from 80 mm onwards, as the impeller diameter approaches the tank wall, an increase in heat transfer effectiveness is observed due to the decrease in thermal boundary layer thickness associated with the increase in hydrodynamic boundary layer thickness in the boundary layer region. The temperature contours are shown in the XZ plane with a sectional view taken through the center of the impeller, as shown in Figures 4.23 and 4.24.

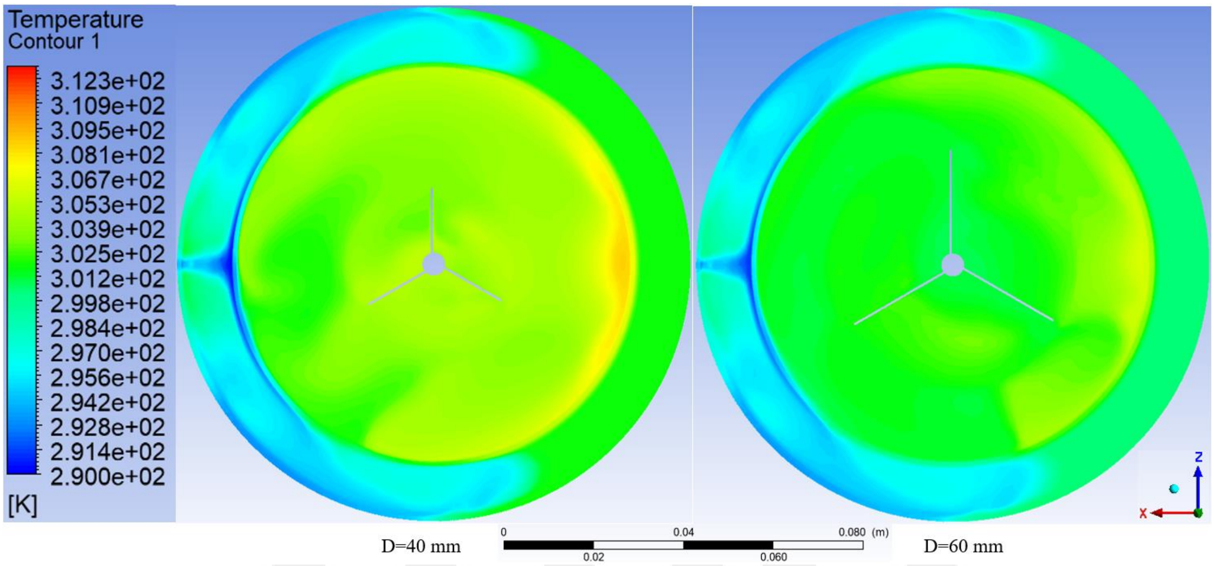

Figure 4.23. Temperature contours for D = 40 mm and D = 60 mm

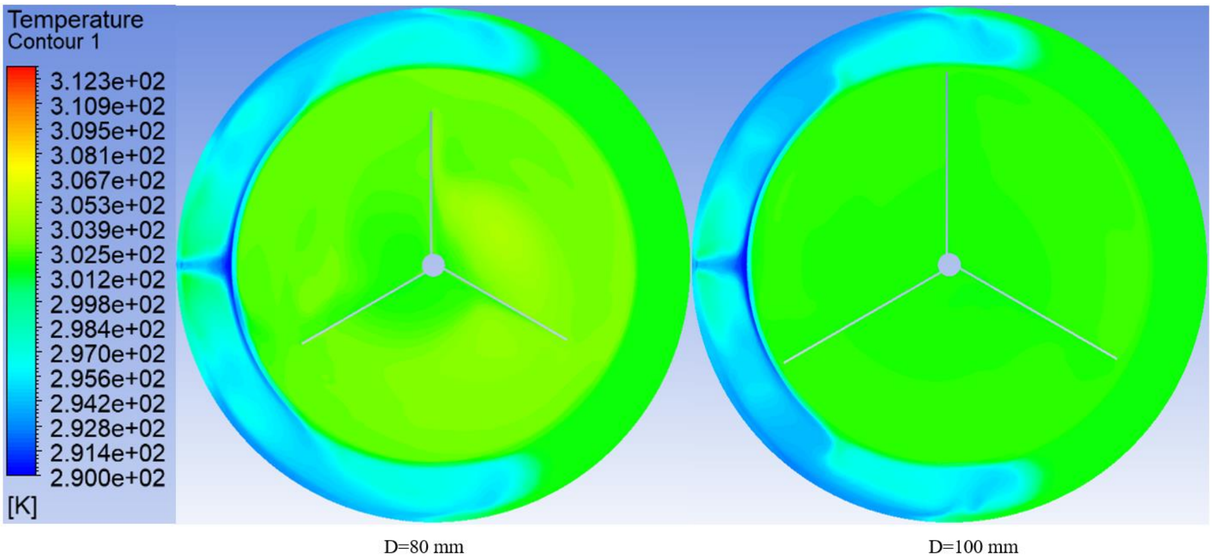

Figure 4.24. Temperature contours for D = 80 mm and D = 100 mm

Larger diameter impellers can provide a more homogeneous temperature distribution and higher heat transfer effectiveness. However, designing without exceeding the optimal diameter at a certain point is important for energy efficiency. The velocity vectors corresponding to these results are presented in Figure 4.25. and 4.26.

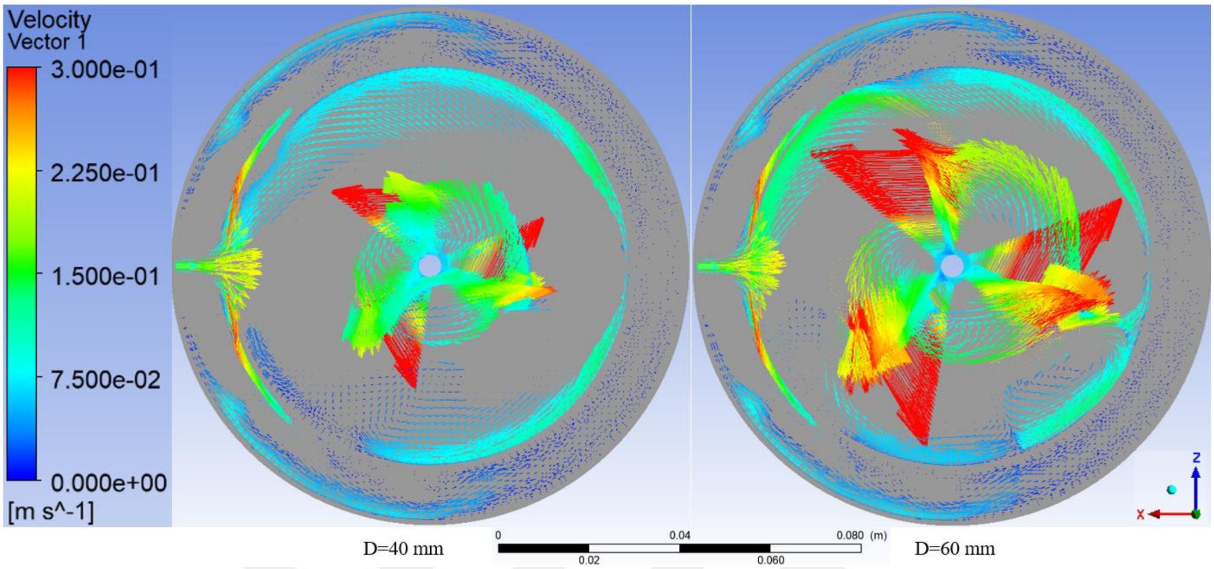

Figure 4.25. Velocity vectors for D = 40 mm and D = 60 mm

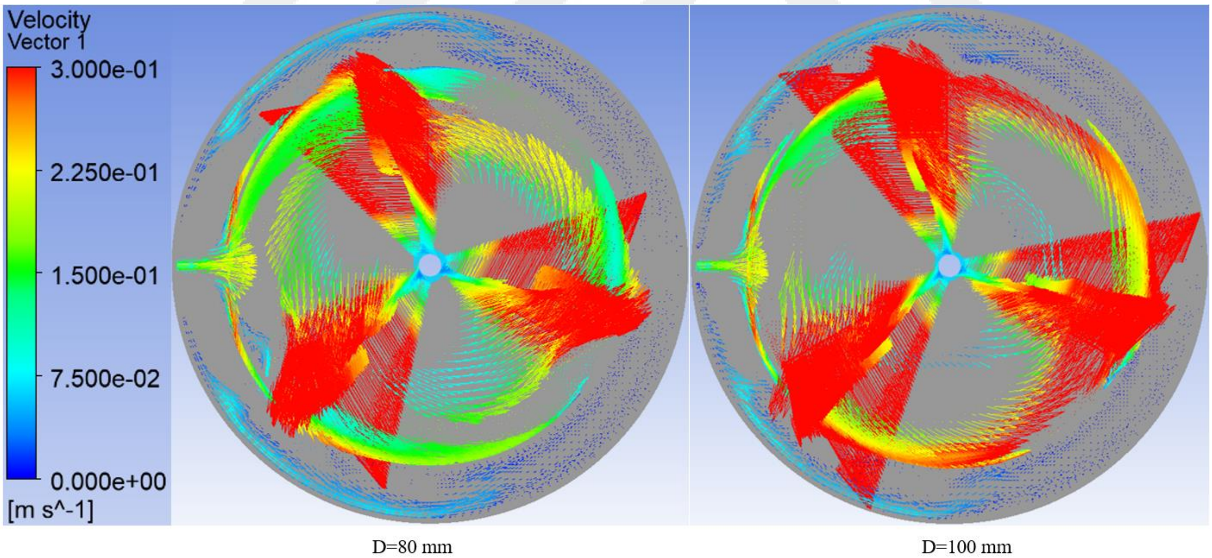

Figure 4.26. Velocity vectors for D = 80 mm and D = 100 mm

As the impeller diameter increases, the velocity vectors and vortex structures become more distinct, and the high-velocity regions expand. This results in better mixing and higher heat transfer effectiveness.

4.2.4. The Effect of Blade Angle on Heat Transfer Performance

In order to examine the effect of the impeller blade angle (θ) on heat transfer performance, the angle between the blade and the vertical y-axis was incrementally (θ = 0°, 15°, 30°, 45°) increased. The parameters kept constant as angular velocity Rev = 100 rpm, impeller diameter D=40 mm, height of the impeller H = 10 mm, number of blade n = 3 and number of stirrer S=1. It was found that changing the angle from 0° to 15° resulted in a 11.8% increase in heat transfer effectiveness, changing it from 15° to 30° resulted in a 0.5% increase, and changing it from 30° to 45° resulted in a 2.1% increase in heat transfer effectiveness. Increasing the blade angle from 0° to 45° resulted in a total increase of 14.4% in heat transfer effectiveness. The effect of blade angle on heat transfer effectiveness is presented in Figure 4.27.

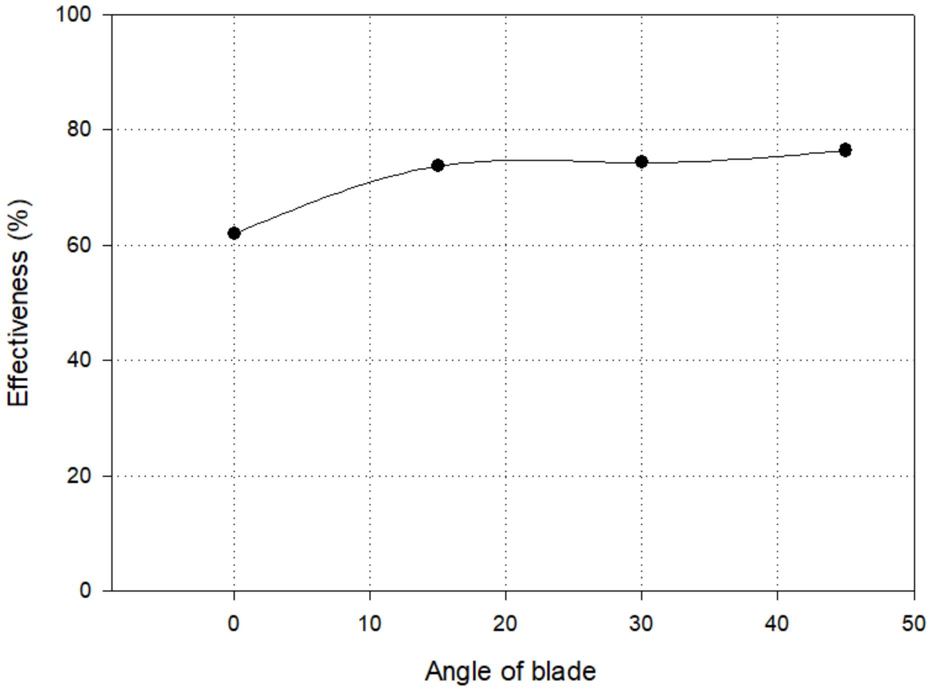

Figure 4.27. The effect of blade angle on heat transfer effectiveness

Increasing the blade angle generally improves temperature uniformity and mixing, especially from θ = 0° to θ = 15°. However, from θ = 15° to θ = 30°, the effectiveness remains nearly constant, suggesting an optimal mixing point. Further increasing the angle to θ = 45° results in a slight improvement in temperature distribution. The temperature contours in the XY plane for four different cases are presented in Figure 4.28., and 4.29.

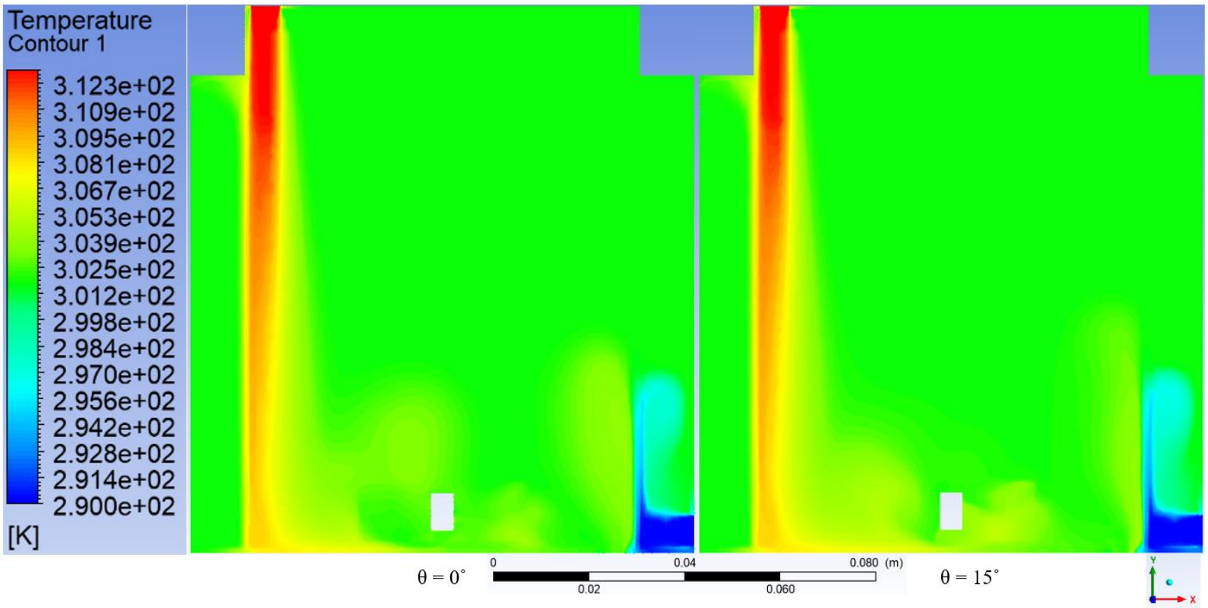

Figure 4.28. The temperature contours for θ=0° and θ=15°

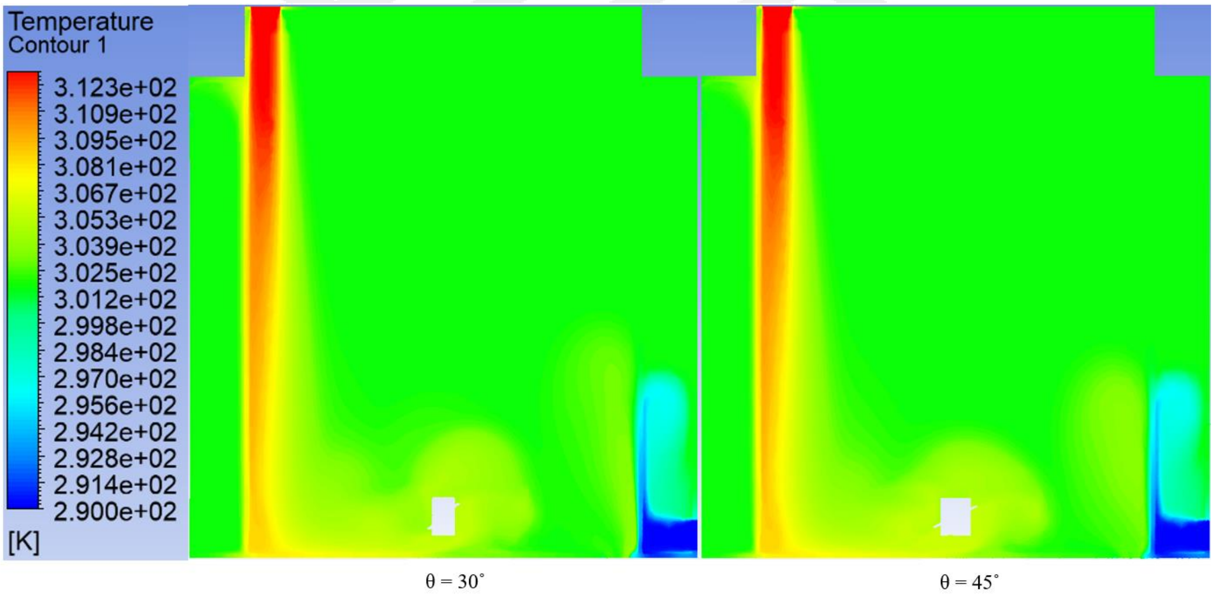

Figure 4.29. The temperature contours for θ=30° and θ=45°

As the blade angle increases from 0° to 15°, the velocity vectors show an increase in turbulence and flow circulation, leading to better mixing. Between 15° and 30°, there is no significant change in the velocity vectors, indicating that the flow has reached an optimal mixing condition. At 45°, the turbulence and circulation slightly increase again, enhancing the mixing effect and heat transfer performance. The velocity vectors for four cases are presented in Figure 4.30. and 4.31.

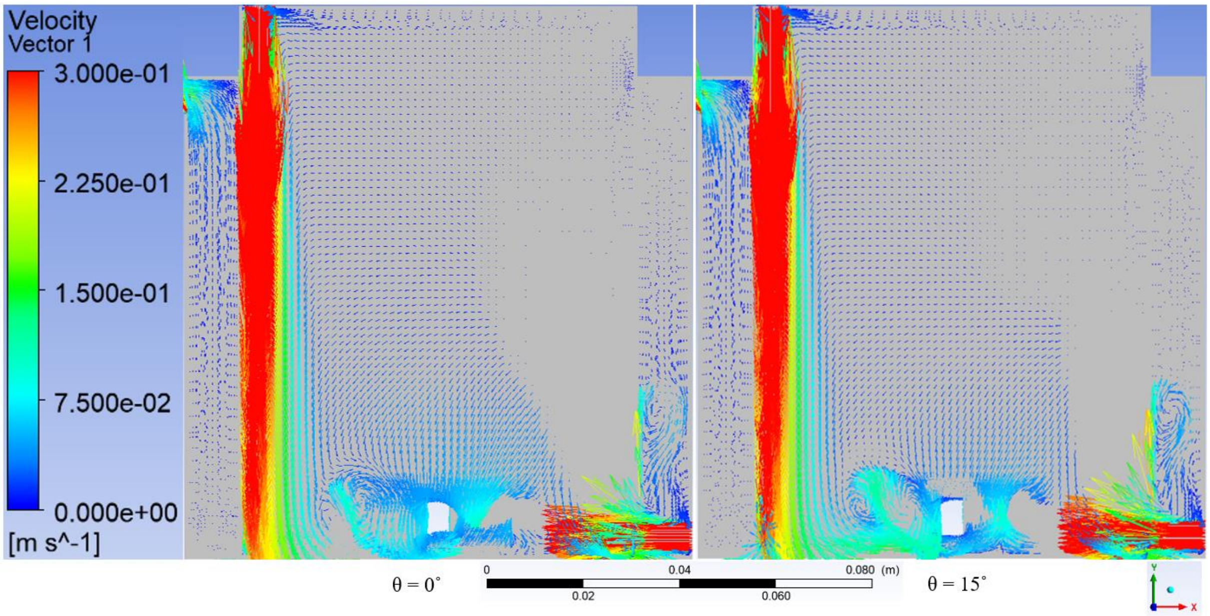

Figure 4.30. The velocity vectors for θ=0° and θ=15°

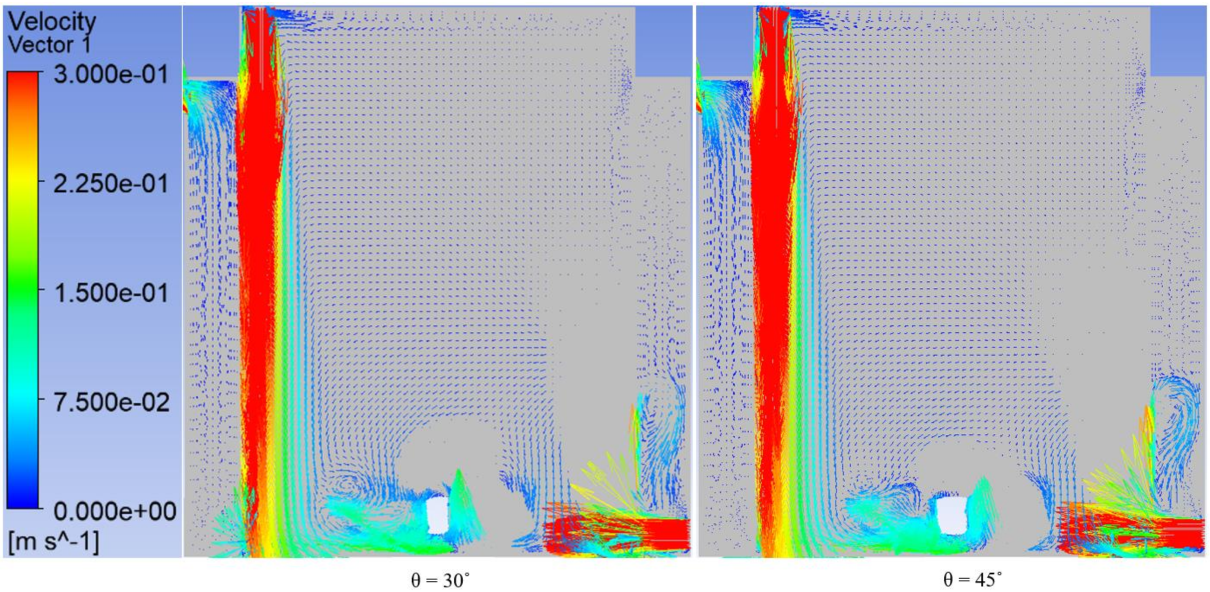

Figure 4.31. The velocity vectors for θ=30° and θ=45°

4.2.5. The Effect of Number of Blades on Heat Transfer Performance

In order to investigate the effect of the number of impeller blades on heat transfer performance in the heat exchanger, the heat transfer effectiveness was examined separately for impellers with different blade numbers. Increasing the number of blades from 2 to 3 resulted in a 12.6% increase in heat transfer effectiveness. Increasing the number of blades from 3 to 5 resulted in a 0.4% decrease and increasing the number from 5 to 7 resulted in a 1.6% decrease in heat transfer effectiveness. When the number of blades is increased beyond this optimal point, the benefits gained from additional mixing and turbulence are outweighed by the drawbacks. Specifically, additional blades can create more flow resistance, which hinders fluid movement and reduces overall efficiency. The increased resistance can disrupt the flow patterns and reduce the impeller's ability to effectively mix the fluid, leading to a decline in heat transfer effectiveness. The effect of blade number on heat transfer effectiveness is presented in Figure 4.32.

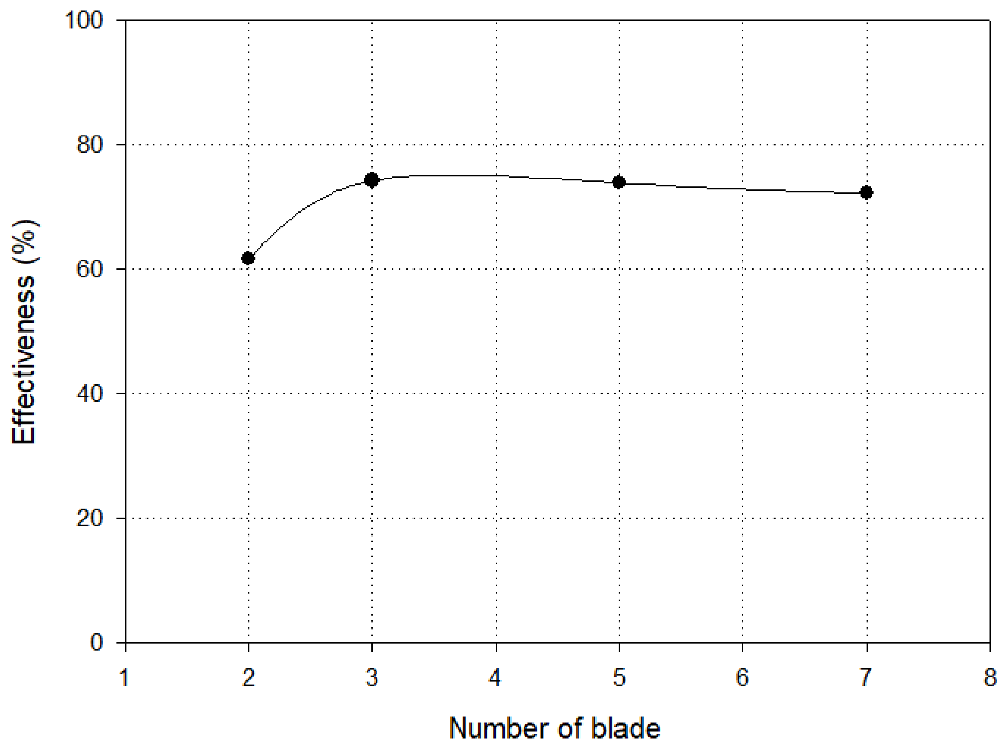

Figure 4.32. The effect of blade number on heat transfer effectiveness

When examining the temperature contours, it is evident that the impeller with 3 blades provides the most uniform temperature distribution. The temperature spread is more even throughout the tank, indicating improved mixing and higher heat transfer effectiveness. The temperature contours are given in Figure 4.33. for different four case.

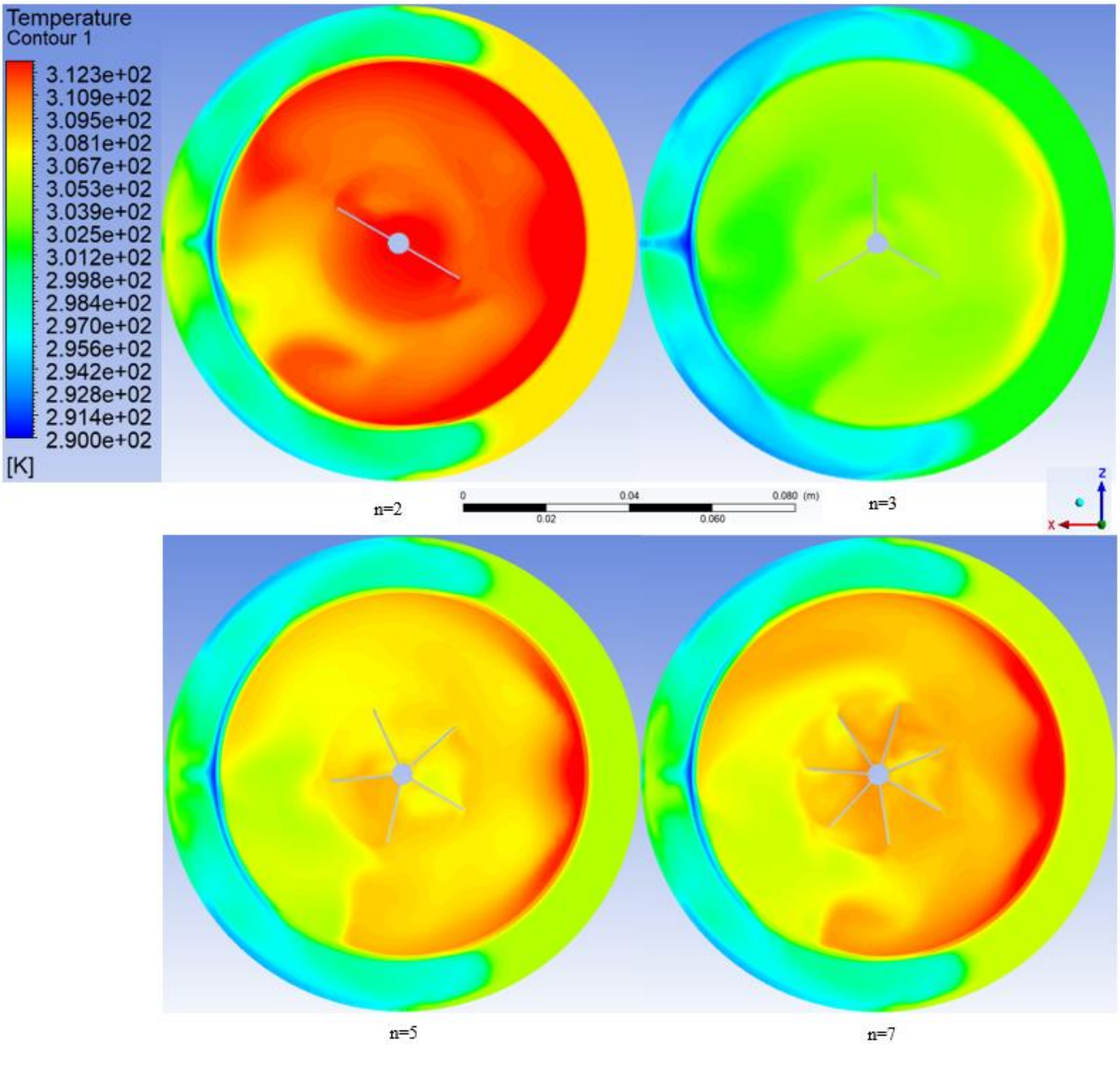

Figure 4.33. The temperature contours for n = 2, n = 3, n = 5, and n = 7

The variation in velocity vectors resulting from an increase in the number of blades is comprehensively illustrated in Figure 4.34. As the number of blades increases, the flow characteristics within the stirred heat exchanger change, affecting both the magnitude and direction of the velocity vectors. This figure provides a detailed depiction of these changes, highlighting how additional blades influence the mixing efficiency and flow dynamics within the system.

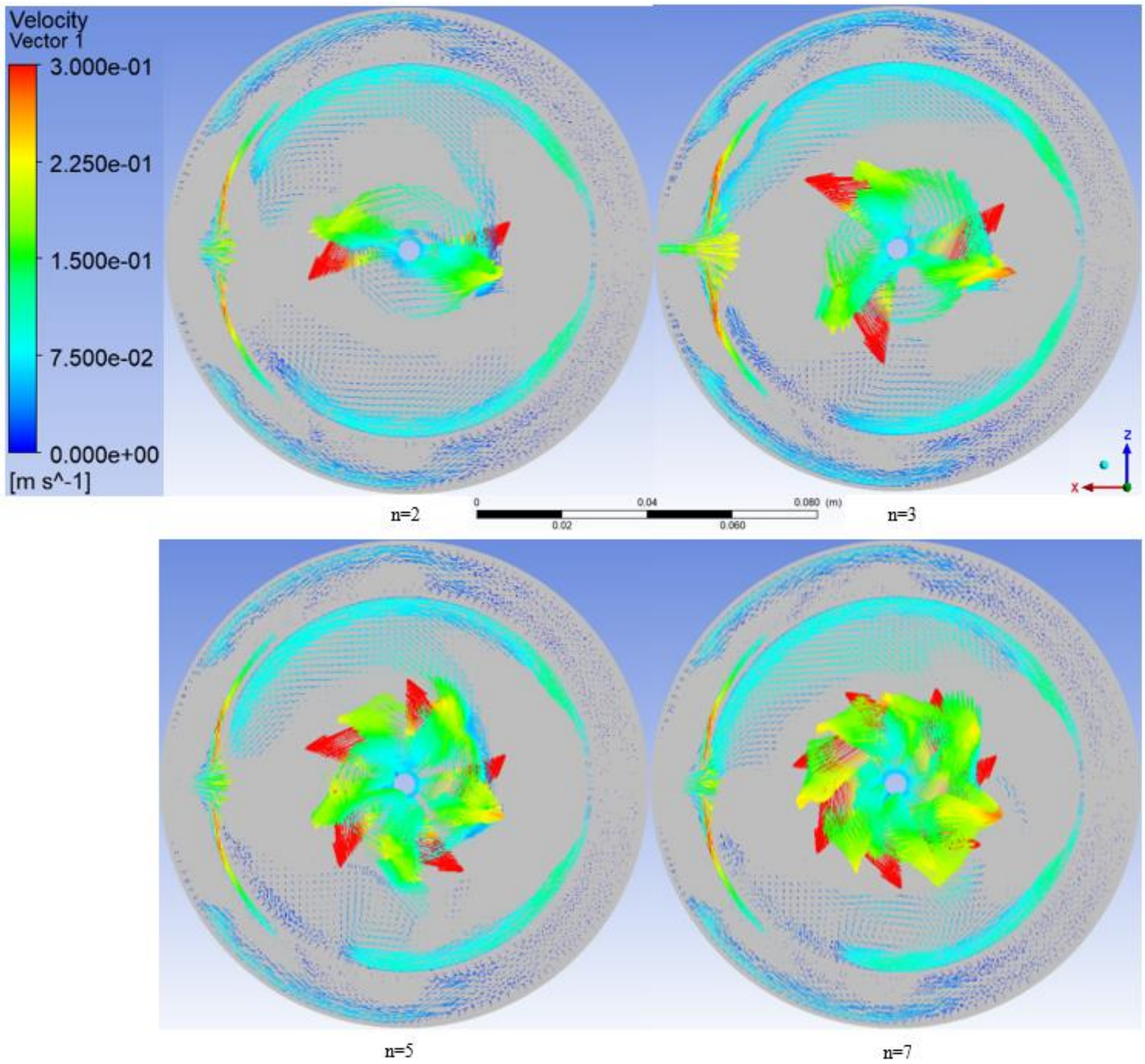

Figure 4.34. The velocity vectors for n = 2, n = 3, n = 5, and n = 7

4.2.6. The Effect of Number of Stirrer on Heat Transfer Performance

To examine the effect of the number of mechanical stirrers on heat transfer performance, the number of stirrers was varied to S = 1, S = 2, and S = 3, spaced evenly along the y-axis within the heat exchanger. With other geometric parameters kept constant, the heat transfer effectiveness of the model with two stirrers was found to be 16.7% higher compared to the model with one stirrer. No significant difference in heat transfer performance was observed between the models with two and three stirrers. This implies that the ideal number of stirrers for optimizing heat transfer effectiveness is two, beyond which additional stirrers give no further advantages. The effect of the number of stirrers on heat transfer performance is presented in Figure 4.35.

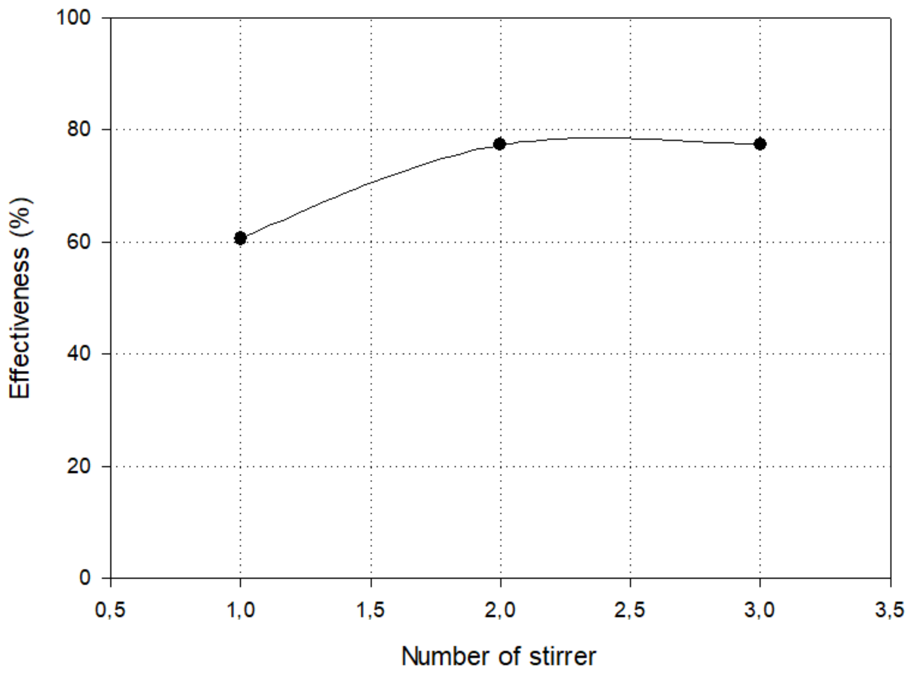

Figure 4.35. The effect of the number of stirrers on heat transfer performance

The addition of a second stirrer significantly improves the uniformity of the temperature distribution, indicating better mixing and higher heat transfer effectiveness compared to a single stirrer configuration. The temperature contours for the configurations with the lowest and highest heat transfer performance, S=1 and S=2, are shown in Figure 4.36.

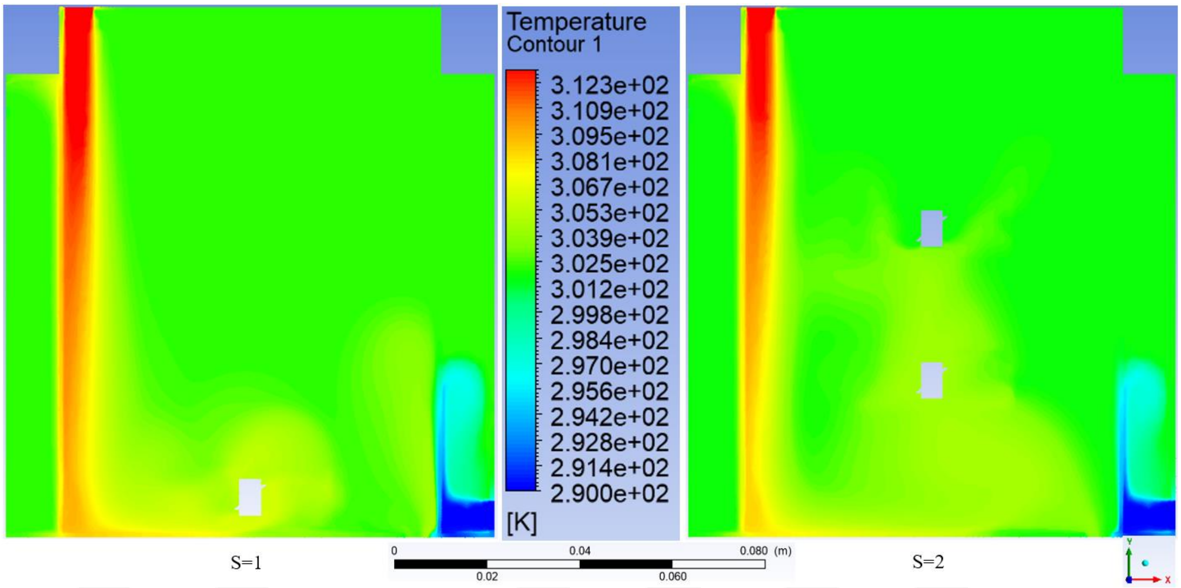

Figure 4.36. The temperature contours for S = 1 and S = 2

The velocity vectors show a more complex and turbulent flow pattern. The presence of two stirrers creates multiple vortices and enhances the circulation throughout the tank. The velocity vectors for the single stirrer and two stirrer cases are shown in Figure 4.37.

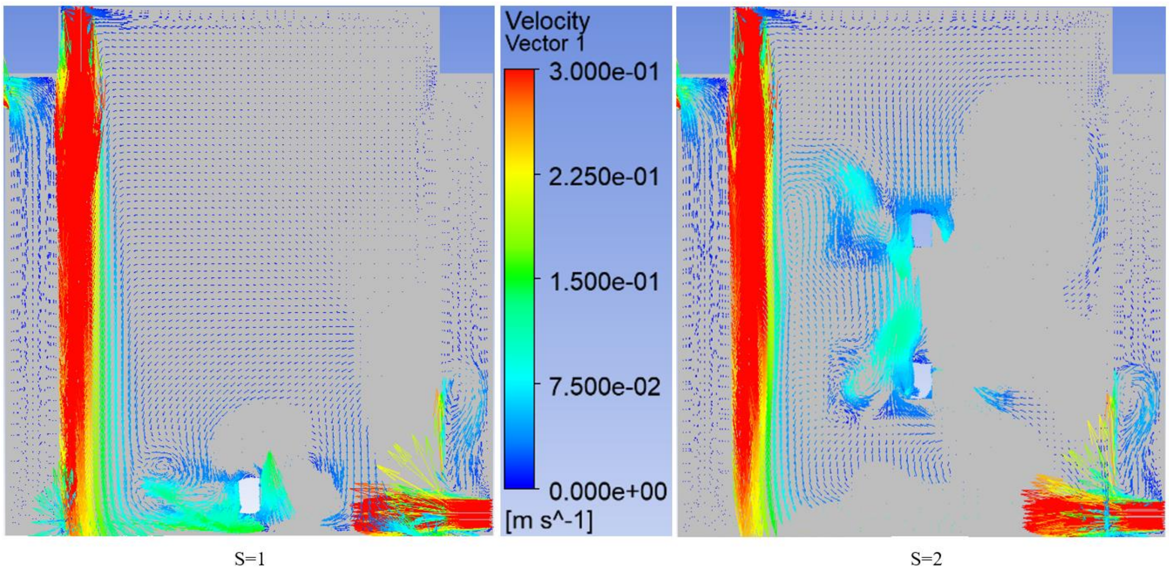

Figure 4.37. The velocity vectors for S = 1 and S = 2

In summary, this study provides a thorough evaluation of the impact of various design and operational parameters on the heat transfer performance of stirred heat exchangers. The experimental and numerical investigations demonstrate that each parameter plays a crucial role in influencing the system's thermal efficiency. Specifically, increasing the impeller diameter enhances the heat transfer rate by promoting better fluid mixing and reducing thermal boundary layer resistance. The number of blades directly affects the turbulence intensity, with more blades generally increasing the turbulence and, consequently, the heat transfer rate, up to an optimal point beyond which further additions may lead to diminishing returns due to increased flow resistance. The blade angle significantly influences the direction and magnitude of fluid flow, where optimal angles improve the mixing efficiency and heat transfer by maximizing shear forces and turbulence. Higher impeller speeds lead to increased Reynolds numbers, which enhance convective heat transfer by promoting greater turbulence and mixing within the tank. The number of stirrers also plays a significant role; while adding a second stirrer enhances mixing and heat transfer efficiency, the addition of a third stirrer does not show a significant improvement, indicating an optimal number for achieving efficient energy transfer. Lastly, varying the Reynolds number, which is a function of flow velocity and characteristic dimensions, was found to have a substantial effect on the overall heat transfer effectiveness, with higher Reynolds numbers generally corresponding to improved heat transfer performance. These findings emphasize the need of optimizing these parameters in stirred heat exchangers to achieve optimum thermal efficiency and uniform temperature distribution, as well as offering significant information for future thermal engineering design and operation methods.

5. CONCLUSIONS

In this thesis study, the effect of the mechanical stirrer's rotational speed, the inlet temperatures of the hot fluid, and the Reynolds number, which is dependent on the fluid velocity, on the heat transfer performance in a stirred heat exchanger was experimentally studied. The numerical model generated in the computational fluid dynamics program of ANSYS 2022 R1 was validated with the experimental model. In the developed numerical model, the rotational speed of the stirrer, the diameter of the impeller, the height of the impeller from the bottom of the heat exchanger, the angle of the blades to vertical y-axis, the number of blades and the number of stirrers were studied. The obtained results from experimental and numerical studies are presented below.

Experimental study results that;

1. Increasing the Reynolds number from Re=4000 to 10000, with the mechanical stirrer in the heat exchanger remaining stationary, resulted in a total increase of 5.6% in heat transfer effectiveness, demonstrating the influence of the Reynolds number on heat transfer performance.

2. When the mechanical stirrer in the heat exchanger rotates at a speed of Rev=100 rpm, a total increase of 4.7% in heat transfer effectiveness was observed when the Reynolds number was increased between Re=4000-10000.

3. When the Reynolds number, dependent on the fluid velocity, is kept constant at Re=6000, a total increase of 49% in heat transfer effectiveness was observed when the stirrer speed was increased in the range of Rev=0-300 rpm to measure the effect of the stirrer speed.

4. To determine the effect of hot fluid inlet temperature on heat transfer performance, increasing the hot fluid inlet temperature in the heat exchanger between 30-55°C resulted in a 5% increase in heat transfer effectiveness.

Numerical study results that;

1. In the heat exchanger, as the rotational speed of the stirrer was increased from 0 to 400 rpm, a total increase of 55.1% in heat transfer effectiveness was observed when the

speed was increased from 0 to 200 rpm. No significant change was recorded beyond 200 rpm.

2. Increasing the impeller height from H=10 mm to H=40 mm resulted in a 17.2% increase in heat transfer effectiveness. However, raising the height to H=70 mm led to a 0.9% decrease, and further increasing the height to H=100 mm caused a 2.8% decrease in heat transfer effectiveness.

3. Increasing the impeller diameter from D=40 mm to D=60 mm resulted in an 11.8% increase in heat transfer effectiveness. When the diameter was increased to D=80 mm, a 0.4% increase was observed, and a further increase to D=100 mm resulted in a 3.75% increase. The overall increase in diameter from 40 mm to 100 mm led to a total increase of 15.9% in heat transfer effectiveness. While an increase in effectiveness is noted as the impeller diameter increases from 40 mm to 60 mm, no increase in effectiveness is detected between 60 mm and 80 mm. This suggests that an optimum has been reached due to the mixing effect caused by fluid dynamics. However, from 80 mm onwards, as the impeller diameter approaches the tank wall, an increase in heat transfer effectiveness is observed due to the reduction in thermal boundary layer thickness associated with the increase in hydrodynamic boundary layer thickness in the boundary layer region.

4. Altering the angle from 0° to 15° led to an 11.8% increase in heat transfer effectiveness. Increasing the angle from 15° to 30° resulted in a 0.5% increase, and from 30° to 45° resulted in a 2.1% increase in heat transfer effectiveness. Increasing the blade angle generally enhances temperature uniformity and mixing, especially from $\theta = 0°$ to $\theta = 15°$. However, between $\theta = 15°$ and $\theta = 30°$, the effectiveness remains nearly constant, suggesting an optimal mixing point. Further increasing the angle to $\theta = 45°$ results in a slight improvement in temperature distribution.

5. Increasing the number of blades from 2 to 3 resulted in a 12.6% increase in heat transfer effectiveness. However, increasing the number of blades from 3 to 5 led to a 0.4% decrease, and from 5 to 7 caused a 1.6% decrease in heat transfer effectiveness. Beyond the optimal number of blades, the advantages of additional mixing and turbulence are offset by drawbacks. Specifically, more blades can create higher flow resistance, which impedes fluid movement and reduces overall efficiency. This increased resistance can

disrupt flow patterns and diminish the impeller's ability to mix the fluid effectively, resulting in a decline in heat transfer effectiveness.

6. The heat transfer effectiveness of the model with two stirrers was 16.7% higher than that of the model with one stirrer. No significant difference in heat transfer performance was observed between the models with two and three stirrers. This indicates that the optimal number of stirrers for maximizing heat transfer effectiveness is two, as additional stirrers beyond this point do not provide further benefits.

7. The findings of this thesis study are likely to be useful in systems utilizing stirred heat exchangers by identifying critical design parameters. These insights can help to create designs that function optimally, resulting in the construction of systems that are more affordable, energy efficient, and capable of providing more effective heat transfer.

8. In future studies in this field, the use of nanofluids as the working fluid in heat exchangers, the addition of turbulators to enhance flow dynamics and vortex formation, and the development of various blade structures to reduce the thermal boundary layer on the tank walls are expected to make significant contributions to the literature.

6. RECOMMENDATIONS

Heat exchangers occupy a significant place in the literature, and with advancing technology, there has been parallel development aimed at improving the heat transfer performance of heat exchangers. Stirred heat exchangers, compared to passive methods, are much less represented in the literature, indicating a gap in this field. Active methods used to enhance efficiency are crucial for achieving more effective heat transfer in small spaces. Future studies in this area are recommended to explore the use of nanofluids to reduce the thermal boundary layer thickness and increase the velocity boundary layer thickness on the heat transfer surface, the use of protruding geometric structures on surfaces, and the effects of magnetic fields on fluids containing ferromagnetic nanoparticles.

REFERENCES

Abolpour, B., Hekmatkhah, R., & Shamsoddini, R. (2021). Multi-objective optimum design for double baffle heat exchangers. *Thermal Science and Engineering Progress*, *26*. https://doi.org/10.1016/j.tsep.2021.101132

Allison, J. M., Staats, W. L., McCarthy, M., Jenicek, D., Edoh, A. K., Lang, J. H., Wang, E. N., & Brisson, J. G. (2011). Enhancement of convective heat transfer in an air-cooled heat exchanger using interdigitated impeller blades. *International Journal of Heat and Mass Transfer*, *54*(21–22), 4549–4559. https://doi.org/10.1016/j.ijheatmasstransfer.2011.06.023

Alwatban, A., & Aljabr, A. (2024). Thermo-flow behavior of air-channel heat exchanger with nonidentical baffle lengths: computational analysis. *Journal of Thermal Analysis and Calorimetry*, *149*(8), 3593–3603. https://doi.org/10.1007/s10973-024-12906-1

B. Lakghomi, E. K. A. J. and F. F. (2006). Coil and Jacket's Effects on Internal Flow Behavior & Heat Transfer in Stirred Tanks. *World Academy of Science, Engineering and Technology 24 2006*, *24*, 147–151. https://citeseerx.ist.psu.edu/document?repid=rep1&type=pdf&doi=229cf7e52386713ad127e7eb821279f37702a5bf

Cengel, Y. A., & Ghajar, A. J. (2020). *Heat and mass transfer : fundamentals and applications* (6th ed.).

Cengel, Y., & Cimbala, J. M. (2014). *Fluid Mechanics* (3rd ed.). McGraw-Hill.

Cui, Y., Zhang, H., Li, X., Yang, M., & Guan, Z. (2018). Computational and experimental investigation of laminar flow mixing system in a pitched-blade turbine stirred tank. *International Journal of Agricultural and Biological Engineering*, *11*(4), 94–101. https://doi.org/10.25165/j.ijabe.20181104.2729

Daza, S. A., Prada, R. J., Nunhez, J. R., & Castilho, G. J. (2019). Nusselt number correlation for a jacketed stirred tank using computational fluid dynamics. *Canadian Journal of Chemical Engineering*, *97*(2), 586–593. https://doi.org/10.1002/cjce.23385

Debab, A., Chergui, N., Bekrentchir, K., & Bertrand, J. (2011). Available online at www.jafmonline.net. In *Journal of Applied Fluid Mechanics* (Vol. 4, Issue 2). www.SID.ir

Delgado, M., Lázaro, A., Mazo, J., Peñalosa, C., Marín, J. M., & Zalba, B. (2017). Experimental analysis of a coiled stirred tank containing a low cost PCM emulsion as a thermal energy storage system. *Energy*, *138*, 590–601. https://doi.org/10.1016/j.energy.2017.07.044

Dhaou, M. H., Mellouli, S., Alresheedi, F., & El-Ghoul, Y. (2022). Experimental assessment of a solar water tank integrated with nano-enhanced PCM and a stirrer. *Alexandria Engineering Journal*, *61*(10), 8113–8122. https://doi.org/10.1016/j.aej.2022.01.040

Di Bari, V., Norton, J. E., & Norton, I. T. (2014). Effect of processing on the microstructural properties of water-in-cocoa butter emulsions. *Journal of Food Engineering*, *122*(1), 8–14. https://doi.org/10.1016/j.jfoodeng.2013.08.036

Fouad, Y. O., Malash, G. F., Zatout, A. A., & Sedahmed, G. H. (2013). Mass and heat transfer at an array of vertical tubes in a square stirred tank reactor. *Chemical Engineering Research and Design*, *91*(2), 234–243. https://doi.org/10.1016/j.cherd.2012.08.006

Gulumyan, A. A., Verigin, A. N., & Lisitsyn, N. V. (2017). Efficiency of mixed-flow heat exchangers. *Theoretical Foundations of Chemical Engineering*, *51*(1), 94–106. https://doi.org/10.1134/S0040579517010079

Hosseini, M. J., Rahimi, M., & Bahrampoury, R. (2014). Experimental and computational evolution of a shell and tube heat exchanger as a PCM thermal storage system. *International Communications in Heat and Mass Transfer*, *50*, 128–136. https://doi.org/10.1016/j.icheatmasstransfer.2013.11.008

Hu, Y., & Heiselberg, P. K. (2018). A new ventilated window with PCM heat exchanger—Performance analysis and design optimization. *Energy and Buildings*, *169*, 185–194. https://doi.org/10.1016/j.enbuild.2018.03.060

Jaehrling, K., & Schultz, H. J. (2019). Flow Fields in Stirred Vessels Depending on Different Internal Heat Exchangers and Vessel Bottoms. *Chemie-Ingenieur-Technik*, *91*(9), 1281–1292. https://doi.org/10.1002/cite.201800101

Joshi, J. B., Nere, N. K., Rane, C. V., Murthy, B. N., Mathpati, C. S., Patwardhan, A. W., & Ranade, V. V. (2011). CFD simulation of stirred tanks: Comparison of turbulence models (Part II: Axial flow impellers, multiple impellers and multiphase dispersions). In *Canadian Journal of Chemical Engineering* (Vol. 89, Issue 4, pp. 754–816). https://doi.org/10.1002/cjce.20465

Karagoz, S., Afshari, F., Yildirim, O., & Comakli, O. (2017). Experimental and numerical investigation of the cylindrical blade tube inserts effect on the heat transfer enhancement in the horizontal pipe exchangers. *Heat and Mass Transfer/Waerme- Und Stoffuebertragung*, *53*(9), 2769–2784. https://doi.org/10.1007/s00231-017-2021-8

Khan, M. S. (2024). Computational heat transfer analysis of liquid food in a heat exchanger with varying stirrer settings in a nonclassical continuum framework. *Numerical Heat Transfer, Part B: Fundamentals*. https://doi.org/10.1080/10407790.2024.2302859

Kisuka, F., Rangel, R. L., Hare, C., Vivacqua, V., & Wu, C. Y. (2023). Experimental investigation of heat generation during the mixing of granular materials using an overhead stirrer. *AIChE Journal*, *69*(12). https://doi.org/10.1002/aic.18219

Luo, X., Yu, J., Wang, B., & Wang, J. (2021). Heat transfer and hydrodynamics in stirred tanks with liquid-solid flow studied by CFD–DEM method. *Processes, 9*(5). https://doi.org/10.3390/pr9050849

Mahir, M., Maakoul, A. El, Khay, I., Saadeddine, S., & Bakhouya, M. (2021). An investigation of heat transfer performance in an agitated vessel. *Processes*, *9*(3), 1–19. https://doi.org/10.3390/pr9030468

Mase, Y., Sucipto, Z. F., & Mobedi, M. (2024). A numerical study on control mechanism of heat transfer in a double pipe PCM heat exchanger by changing eccentricity. *Energy, 291*. https://doi.org/10.1016/j.energy.2024.130266

Mohan Anthony Nicholas Emery Tariq AI-Hassan, P. (1992). *Review Heat Transfer to Newtonian Fluids in Mechanically Agitated Vessels*.

Niedbalski, N., Johnson, D., Patnaik, S. S., & Banerjee, D. (2014). Study of a multi-phase hybrid heat exchanger-reactor (HEX reactor): Part I – Experimental characterization. *International Journal of Heat and Mass Transfer*, *70*, 1078–1085. https://doi.org/10.1016/j.ijheatmasstransfer.2013.10.066

Nobuo Mitsuishi, Y. M. (1973). Heat Transfer To Non-Newtonian Fluids In An Agitated Vessel. *Journal of Chemical Engineering of Japan*, *6*, 415–420.

Norton, J. E., & Fryer, P. J. (2012). Investigation of changes in formulation and processing parameters on the physical properties of cocoa butter emulsions. *Journal of Food Engineering*, *113*(2), 329–336. https://doi.org/10.1016/j.jfoodeng.2012.05.025

Parsa, N., Kamkari, B., & Abolghasemi, H. (2024). Experimental study on the influence of shell geometry and tube eccentricity on phase change material melting in shell and tube heat exchangers. *International Journal of Heat and Mass Transfer, 227*. https://doi.org/10.1016/j.ijheatmasstransfer.2024.125571

Patil, H., Patel, A. K., Pant, H. J., & Venu Vinod, A. (2021). CFD simulation model for mixing tank using multiple reference frame (MRF) impeller rotation. *ISH Journal of Hydraulic Engineering*, *27*(2), 200–209. https://doi.org/10.1080/09715010.2018.1535921

Paul, E. L., Atiemo-Obeng, V. A., & Kresta, S. M. (2004a). *Handbook of industrial mixing : science and practice*. Wiley-Interscience.

Paul, E. L., Atiemo-Obeng, V. A., & Kresta, S. M. (2004b). *Handbook of industrial mixing : science and practice*. Wiley-Interscience.

Paul, E. L., Atiemo-Obeng, V. A., & Kresta, S. M. (2004c). *HANDBOOK OF INDUSTRIAL MIXING SCIENCE AND PRACTICE Edited by*. www.copyright.com.

Petera, K., Dostál, M., Jirout, T., & Fořt, I. (2016). Heat transfer similarities between impinging jets and axial-flow impellers. *Theoretical Foundations of Chemical Engineering*, *50*(6), 937–944. https://doi.org/10.1134/S0040579516060130

Rasslan, W. B., Abdel-Kawi, M. A., Nosier, S. A., El-Maghlany, W. M., Abdel-Aziz, M. H., Sedahmed, G. H., & Fathalla, A. S. (2023). Experimental mass and heat transfer at a serpentine tube heat exchanger located at the wall of a square stirred tank reactor. *Applied Thermal Engineering*, *219*. https://doi.org/10.1016/j.applthermaleng.2022.119438

Rezend, C. (1996a). *CFD analysis of flow field in a mixing tank with and without baffles*. https://repository.rit.edu/theses

Rezend, C. (1996b). *CFD analysis of flow field in a mixing tank with and without baffles*. https://repository.rit.edu/theses

Safari, V., Kamkari, B., & Gharbi, A. (2024). Wedge-shaped fins to enhance thermal performance of shell and tube heat exchangers containing phase change material: An experimental study. *Thermal Science and Engineering Progress*, *49*. https://doi.org/10.1016/j.tsep.2024.102474

Sevilgen, G., & BAYRAM, H. (2018). Bir gövde borulu ısı değiştiricisinde farklı levha türlerinin ısıl performansa etkisinin sayısal olarak incelenmesi. *Academic Platform Journal of Engineering and Science*, 1–1. https://doi.org/10.21541/apjes.397414

Shen, Y. Y., Qin, B., Li, X., Zhu, Z., Cui, P., Gao, J., & Wang, Y. (2021). Investigation of the flow characteristics of liquid–liquid two-phase mixing in an agitator equipped with a "V-shaped" horizontal baffle. *Environment, Development and Sustainability*, *23*(2), 2298–2313. https://doi.org/10.1007/s10668-020-00675-4

Soliman, M. S., Nosier, S. A., Hussein, M., Sedahmed, G. H., & Mubarak, A. A. (2017). Mass and heat transfer behavior of a new heterogeneous stirred tank reactor with serpentine tube baffles. In *Chemical Engineering Research and Design* (Vol. 124, pp. 211–221). Institution of Chemical Engineers. https://doi.org/10.1016/j.cherd.2017.06.012

Srinivas, T., & Venu Vinod, A. (2013). Performance of an agitated helical coil heat exchanger using Al2O3/water nanofluid. *Experimental Thermal and Fluid Science*, *51*, 77–83. https://doi.org/10.1016/j.expthermflusci.2013.07.003

Srinivas, T., & Venu Vinod, A. (2015). Heat Transfer Enhancement using CuO / Water Nanofluid in a Shell and Helical Coil Heat Exchanger. *Procedia Engineering*, *127*, 1271–1277. https://doi.org/10.1016/j.proeng.2015.11.483

Srinivas, T., & Venu Vinod, A. (2016). Heat transfer intensification in a shell and helical coil heat exchanger using water-based nanofluids. *Chemical Engineering and Processing: Process Intensification*, *102*, 1–8. https://doi.org/10.1016/j.cep.2016.01.005

Sui, Y., Jiang, W., Zhang, D., Meng, H., & Zhao, Y. (2024). Effect of off-bottom clearance of Lightnin impeller on heat transfer performance in the stirred tank coupled with draft tube. *International Journal of Heat and Mass Transfer*, *225*. https://doi.org/10.1016/j.ijheatmasstransfer.2024.125401

Zhang, X. Y., Ge, Y. T., Burra, & Lang, P. Y. (2024). Experimental investigation and CFD modelling analysis of finned-tube PCM heat exchanger for space heating. *Applied Thermal Engineering*, *244*. https://doi.org/10.1016/j.applthermaleng.2024.122731

Zhao, S., Guo, J., Dang, X., Ai, B., Zhang, M., Li, W., & Zhang, J. (2022). Energy consumption, flow characteristics and energy-efficient design of cup-shape blade stirred tank reactors: Computational fluid dynamics and artificial neural network investigation. *Energy*, *240*. https://doi.org/10.1016/j.energy.2021.122474